JOURNAL OF GEOPHYSICAL RESEARCH, VOL. 113, D10203, doi:10.1029/2007JD009414, 2008

Sensitivity of multiangle imaging to the optical and microphysical properties of biomass burning aerosols

Wei-Ting Chen,[1] Ralph A. Kahn,[2,3] David Nelson,[2] Kevin Yau,[2] and John H. Seinfeld[1,4]

Received 24 September 2007; revised 14 January 2008; accepted 23 January 2008; published 28 May 2008.

[1] The treatment of biomass burning (BB) carbonaceous particles in the Multiangle Imaging SpectroRadiometer (MISR) Standard Aerosol Retrieval Algorithm is assessed, and algorithm refinements are suggested, based on a theoretical sensitivity analysis and comparisons with near-coincident AERONET measurements at representative BB sites. Over the natural ranges of BB aerosol microphysical and optical properties observed in past field campaigns, patterns of retrieved Aerosol Optical Depth (AOD), particle size, and single scattering albedo (SSA) are evaluated. On the basis of the theoretical analysis, assuming total column AOD of 0.2, over a dark, uniform surface, MISR can distinguish two to three groups in each of size and SSA, except when the assumed atmospheric particles are significantly absorbing (mid-visible SSA ~0.84), or of medium sizes (mean radius ~0.13 μm); sensitivity to absorbing, medium-large size particles increases considerably when the assumed column AOD is raised to 0.5. MISR Research Aerosol Retrievals confirm the theoretical results, based on coincident AERONET inversions under BB-dominated conditions. When BB is externally mixed with dust in the atmosphere, dust optical model and surface reflection uncertainties, along with spatial variability, contribute to differences between the Research Retrievals and AERONET. These results suggest specific refinements to the MISR Standard Aerosol Algorithm complement of component particles and mixtures. They also highlight the importance for satellite aerosol retrievals of surface reflectance characterization, with accuracies that can be difficult to achieve with coupled surface-aerosol algorithms in some higher AOD situations.

Citation: Chen, W.-T., R. A. Kahn, D. Nelson, K. Yau, and J. H. Seinfeld (2008), Sensitivity of multiangle imaging to the optical and microphysical properties of biomass burning aerosols, *J. Geophys. Res.*, *113*, D10203, doi:10.1029/2007JD009414.

1. Introduction

[2] Satellite remote sensing provides frequent, long-term global monitoring for tropospheric aerosols. The Multiangle Imaging SpectroRadiometer (MISR) aboard the NASA Earth Observing System (EOS) Terra satellite contributes a great deal of information about aerosol characteristics through its multiangle, multispectral measurements. MISR images Earth at nine view angles (nadir plus 26.1°, 45.6°, 60.0°, and 70.5° in the forward and aft directions along the spacecraft track) and in four spectral bands (446, 558, 672, and 867 nm). Operational since early 2000, MISR observes Earth successively along a ~360 km wide swath and obtains global coverage once in nine days at the Equator with a spatial resolution of 275 m to 1 km. The retrieval products include land surface, cloud, and aerosol properties [*Diner et al.*, 1998].

[3] Deriving aerosol microphysical properties is a major objective of the MISR program. The MISR Standard Aerosol Retrieval Algorithm obtains aerosol optical depth (AOD) and aerosol type at a resolution of 17.6 km, by analyzing MISR top-of-atmosphere radiances from 16 × 16 pixel patches of 1.1-km resolution [*Diner et al.*, 2001]. To systematically improve the MISR Standard Retrieval Algorithm, which automatically processes all the MISR data, it is necessary to explore in greater detail the properties of individual aerosol components. A series of theoretical studies was carried out to assess the multidimensional sensitivity of the MISR aerosol retrieval algorithm prior to launch. Observed radiances over cloud-free, dark water conditions were simulated by systematically varying aerosol optical depths (AODs) and microphysical properties (generic retrievals) [*Kahn et al.*, 1997, 1998] or by varying the proportions of multicomponent aerosol mixtures (climatological retrievals) [*Kahn et al.*, 2001], to determine the ranges of component model properties giving acceptable matches to the measurements. The generic retrievals, in which the aerosol population is specified by monomodal, lognormal size distributions of uniform composition, dem-

[1]Department of Environmental Science and Engineering, California Institute of Technology, Pasadena, California, USA.
[2]Jet Propulsion Laboratory, California Institute of Technology, Pasadena, California, USA.
[3]Now at NASA Goddard Space Flight Center, Greenbelt, Maryland, USA.
[4]Department of Chemical Engineering, California Institute of Technology, Pasadena, California, USA.

0148-0227/08/2007JD009414$09.00

onstrated the capability to distinguish aerosols in three to five size groups, two to four compositional groups (by single scattering albedo) [*Kahn et al.*, 1998], and spherical versus nonspherical shape [*Kahn et al.*, 1997], under average viewing conditions. In addition, the climatological retrievals, in which the aerosol is assumed to be an external mixture consisting of various fractions of component particles having fixed microphysical properties, are able to identify mixtures containing typical sea salt, dust, and black carbon to within 20 percent or better of each component's AOD fraction; maritime and continental aerosol air masses can also be distinguished. Total optical depth is constrained to at least 0.05 or 20 percent, whichever is larger; however, particle microphysical property information in the MISR data decreases for AOD below about 0.15 to 0.2 [*Kahn et al.*, 2001, 2005a].

[4] Carbonaceous particles emitted by biomass burning (BB) activities are one of the tropospheric aerosol species that pose great challenges to climate study. The Intergovernmental Panel on Climate Change (IPCC) estimated the global, annual average direct radiative forcing of BB aerosols to be $+0.03 \pm 0.12$ W/m^2, but the level of scientific understanding is considered low [*Forster et al.*, 2007], and the regional, seasonal impact can be much higher and more uncertain. BB aerosol emissions in the Northern Hemisphere are concentrated in India, Southern China, and Southeast Asia, usually peaking from March to April, in North American boreal forest from June to September, and also in the Sahel region (West Africa) from November to March. Intense BB in the Southern Hemisphere occurs from August to October, mostly in the Amazonian forest of South America and in Tropical and Southern Africa [*Duncan et al.*, 2003], and from October to January in Australia. Large burning events also occur in boreal forest and dry grassland due to lightning, abnormal droughts, or arson, such as the Siberian forest fires in 1997, the tropical rain forest fire in Indonesia from 1997 to 1998, and the Southern California fires in October 2003 and 2007. It is estimated that about 25.0 Tg of primary organic carbon and 3.3 Tg of black carbon is released annually by BB [*Bond et al.*, 2004; *Andreae and Merlet*, 2001]. Improved knowledge of BB smoke properties, amounts, and spatial distribution globally, to which MISR observations can contribute, will enhance current understanding of the role BB particles play in climate, regional visibility, and public health.

[5] Validation with AERONET AOD measurements shows that, over BB sites during the peak of burning season, MISR AOD (version 12) generally exhibits a low bias with large uncertainty; adding to the algorithm climatology more absorbing spherical particle components is suggested to reduce the discrepancies [*Kahn et al.*, 2005a]. However, MISR aerosol property retrievals over BB regions have never been validated with great details. Therefore in this study we aim to suggest refinements to the BB particle models assumed in the current MISR Standard Aerosol Algorithm, by assessing the sensitivity of MISR to BB aerosol properties, through a combination of theoretical analyses and data retrieval studies.

[6] The paper is organized as follows: the strengths and limitations of Version 17 MISR Standard Aerosol retrievals are assessed, by comparing coincident MISR and AErosol RObotic NETwork (AERONET) measurements at sites in major BB regions during the year 2001 burning season. This motivates the work presented in subsequent sections. To identify BB aerosol components missing from the Standard algorithm, recently published data on BB aerosols, especially physical and optical parameters, are summarized briefly in section 3. On the basis of the summarized data, a set of 16 BB particle component models is selected to to represent natural BB smoke type, and the ability of MISR to distinguish among them is explored theoretically in section 4. MISR Research Aerosol Retrievals are carried out in section 5 for representative cases chosen from section 2, using the BB components identified in section 3, and detailed surface characterization. The results and discussions are summarized in the final section.

2. Near-Coincident MISR-Aeronet Measurements in Major BB Regions

2.1. Data Selection

[7] To understand the performance of MISR retrievals over land for ambient BB particles, near-coincident MISR and AERONET events at eight AERONET sites located in major BB regions are analyzed (Table 1). MISR Standard Aerosol Retrieval products, version 17, from December 2000 through August 2001, are compared in this study with AERONET version 2, level 1.5 measurements. These data cover the entire burning season in W. Africa and part of the burning season in S. Africa and S. America, providing typical BB cases in these regions. To ensure meaningful comparisons of particle microphysical properties, only those cases with mid-visible AERONET AOD larger than 0.15 are taken for the analysis. There are 24 qualifying, coincident cases over this period, for which the locations are listed in Table 1. Available AERONET direct sun AOD measurements within ±1 hour, and single scattering albedo (SSA, the ratio of the scattering efficiency to the total extinction efficiency) and size distribution almucantar inversions within ±2 h of MISR overflight are averaged. Spectral AOD and SSA are interpolated linearly between the nearest AERONET channel pairs to the MISR channel effective wavelengths.

[8] MISR Standard Aerosol Retrieval Algorithm compares the observed top-of-atmosphere (TOA) radiance for the MISR channels with a database of simulated radiances. The radiance database is developed by assuming a range of candidate aerosol mixtures and optical depths. The mixtures consist of three component particle optical models with specified component fractions, and each component has unique microphysical properties, representing some part of the range of size distributions, spectral SSA, and sphericity found in naturally occurring aerosols [*Diner et al.*, 2001]. Several χ^2 tests are used to assess the degree to which observed radiances match modeled radiances. AOD and aerosol type are retrieved based on those mixtures from the database that meet the acceptance criteria [e.g., *Kahn et al.*, 2001].

[9] AERONET is a globally distributed remote sensing network of automated Sun-sky scanning CIMEL radiometers [*Holben et al.*, 1998], providing daily ground-based observations of spectral AOD. Because standardized instrumentation, calibration, and retrieval algorithms are used in the entire network, AERONET data are suitable for com-

Table 1. AERONET Sites in Major BB Regions Selected for Coincident MISR-AERONET Measurement Comparisons

Site	Lat.	Lon.	Alt., m	# of All Cases	# of $\tau_{558} > 0.15$ Cases
W. Africa					
Banizoumbou	13.53	2.67	250	7	5
Ilorin	8.32	4.33	350	5	5
Ouagadougou	12.18	−1.38	290	7	7
S. Africa					
Mongu	−15.25	23.15	1107	3	1
Skukuza	−24.98	31.58	150	8	3
S. America					
Alta Floresta	−9.92	−56.02	175	0	0
Belterra	−2.65	−54.95	70	1	1
Cuiaba-Miranda	−15.72	−56.02	210	2	2
				(total = 33)	(total = 24)

parisons across different regions [*Dubovik et al.*, 2002]. AERONET AOD measurements and aerosol property inversions serve as useful references for MISR retrieval validation, but we note that AERONET-retrieved particle properties come with greater uncertainties than AERONET AOD values. Uncertainty of AERONET AOD is generally within 0.01–0.02 [*Holben et al.*, 1998], whereas for BB aerosols with high AOD ($AOD_{440} > 0.5$), the error of AERONET volume size distribution and SSA is estimated to be around 25% and 0.03, respectively, and the error increases significantly with lower aerosol loading, especially for SSA. The uncertainties of AERONET particle property retrievals are mainly related to the error in angular pointing and the inaccuracy in accounting for ground reflectance [*Dubovik et al.*, 2000; *Sinyuk et al.*, 2007].

2.2. Comparison of Near-Coincident MISR-AERONET BB Cases

[10] Figure 1a shows the AERONET mid-visible AOD (hereafter AOD_A) and mid-visible SSA (hereafter SSA_A) for all 24 qualifying cases. In general, when the aerosols are absorbing (SSA_A = 0.80–0.90), mid-visible AOD is smaller than 0.6, whereas in the less absorbing to weakly absorbing cases (SSA_A = 0.90–0.99), mid-visible AOD can be as low as 0.17 and as high as 1.74. Figure 1b shows the difference of AOD between MISR v17 and AERONET data ($AOD_{M\text{-}A}$) against AOD_A. MISR v17 AOD (AOD_M) shows small and unbiased deviation (within ±20%) with respect to AERONET when AOD_A is below 0.5. In cases with $AOD_A > 0.5$, AOD_M is apparently underestimated; in some extreme cases with AOD_A around 1.5 to 1.7, the differences can be as significant as −0.7 to −1. Figure 1c plots SSA_A versus the MISR-AERONET SSA differences ($SSA_{M\text{-}A}$). The overestimation of SSA by the MISR v17 Standard Algorithm (SSA_M) is pervasive, and increases as the atmosphere becomes more absorbing. The discrepancies increase from +0.05 when SSA_A is 0.9 to as much as +0.15 when SSA_A is 0.80. That is, SSA_M is pretty close to unity for all cases, whereas SSA_A varies between 0.8 and 1.0.

[11] To explore this behavior further, we separate the cases into four distinct groups based on the patterns of differences in AOD, SSA, Ångstrom Exponent ($\mathring{A}$), and SSA spectral dependence (α_{ω_0}). The relevant quantities are plotted in Figures 1d–1h. The wavelength dependence of SSA is defined by fitting the spectral SSA to the power law relationship,

$$\omega_0(\lambda) \propto \lambda^{-\alpha_{\omega_0}}, \tag{1}$$

and α_{ω_0} is calculated as the slope of the linear regression of the logarithm:

$$\ln \omega_0(\lambda_i) = a_0 - \alpha_{\omega_0} \ln \lambda_i, \tag{2}$$

where λ_i's represent discrete channels measured by the instruments, and a_0 is a constant. This is similar to the manner in which the Ångstrom Exponent represents the spectral slope of AOD. On the basis of field measurement data, BB particles generally exhibit positive α_{ω_0} values (i.e., decreasing SSA with increasing wavelength); this will be discussed in detail in section 3.

[12] Figures 1e and 1f show that Group 1 (black diamonds) is distinguished by high Ångstrom Exponent and high SSA spectral dependence. Further, Groups 2 (red triangles), 3 (green rectangles), and 4 (yellow circles) differ in their mid-visible AOD and SSA ranges. The four case groupings, along with the regional and seasonal distribution of cases, are summarized in Table 2. Most cases occur during the major burning season of each region, but no significant seasonal differences can be identified with the limited data set of cloud-free coincidences available. Group 1 includes cases from South America and Southern Africa, whereas the events of the other three groups are located exclusively in W. Africa.

[13] MISR v17 AOD number fractions of spherical particles are also examined for the four case groups, as listed in Table 2. Groups 1 and 2 have higher fractional contribution to AOD by spherical particles (between 0.8 to 1.0), whereas groups 3 and 4 exhibit a wide range of spherical fractions (0.2 to 0.6 for group 3; 0.5 to 1.0 for group 4). The 48-h back trajectories at 0.5 km, 1.5 km, and 3 km altitude calculated by the NOAA HYbrid Single-Particle Lagrangian Integrated Trajectory (HYSPLIT) model [*Draxler and Rolph*, 2003] (not shown) suggest that the Group 1 cases have clean continental or maritime air mass origins, whereas in the other groups, 12 of the 16 W. Africa cases have air masses that passed over the Sahara before reaching the fire region. The higher MISR aerosol sphericity fraction, more absorbing SSA, larger Ångstrom Exponent, noticeably steeper and positive SSA spectral slopes, and air mass

Figure 1. Comparisons among coincident MISR-AERONET BB cases with mid-visible AOD > 0.15: (a) AERONET mid-visible AOD (AOD_A) versus SSA (SSA_A), (b) AOD_A versus difference in AOD ($AOD_{M\text{-}A}$), (c) SSA_A versus difference in SSA ($SSA_{M\text{-}A}$), (d) $AOD_{M\text{-}A}$ versus $SSA_{M\text{-}A}$, (e) AERONET Ångstrom Exponent ($\mathring{A}_A$) versus $AOD_{M\text{-}A}$, (f) AERONET SSA spectral dependence ($\alpha_{\omega_{0A}}$) versus SSA_A, (g) $\mathring{A}_A$ versus difference in Ångstrom Exponent ($\mathring{A}_{M\text{-}A}$), (h) $\alpha_{\omega_0}A$ versus difference in SSA spectral dependence ($\alpha_{\omega_{0M\text{-}A}}$). In each panel, cases are categorized into four groups (see text for details): black diamonds for group 1, red triangles for group 2, green squares for group 3, and yellow circles for group 4.

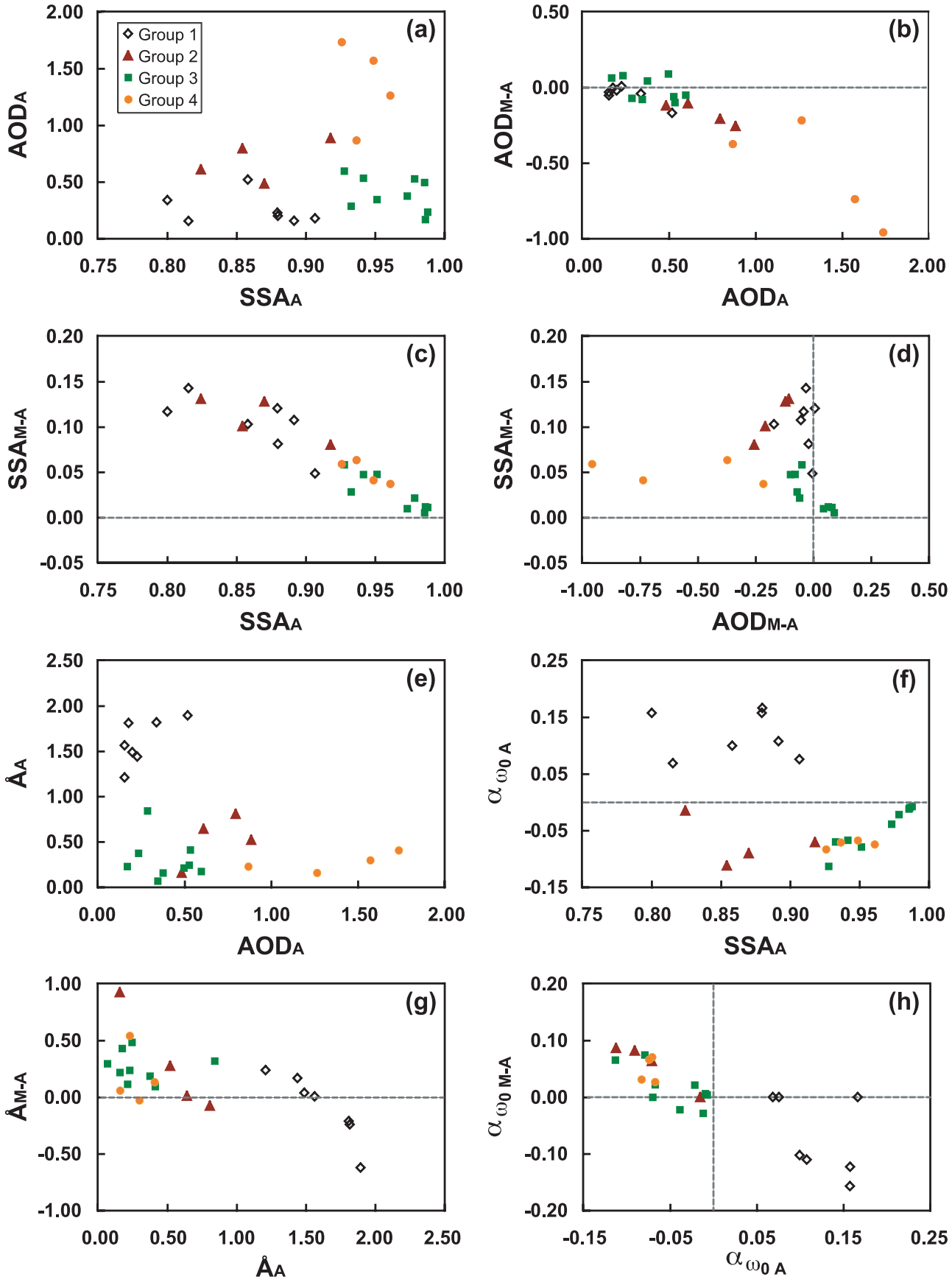
(a)
Group 1
Group 2
Group 3
Group 4
AODA
SSAA
(b)
AODM-A
AODA
(c)
SSAM-A
SSAA
(d)
SSAM-A
AODM-A
(e)
ÅA
AODA
(f)
α ω0 A
SSAA
(g)
ÅM-A
ÅA
(h)
α ω0 M-A
α ω0 A

Figure 1

Table 2. Characteristics of Four Groups of BB Cases, Based on Comparisons of AOD and SSA for Coincident MISR-AERONET Measurements

Group	Location–Season (# of Cases)	MISR-AERONET Comparison	Ambient Aerosol	Possible Reason for MISR Discrepancies
1	S America–Aug (3) S. Africa–Mar, Jun, Aug (4) (total = 7 cases)	AOD_A = 0.2∼0.5; $AOD_{M\text{-}A}$ = −0.17∼0 $\mathring{A}_A$ = 1.4∼1.9; $\mathring{A}_{M\text{-}A}$ = −0.6∼+0.2 SSA_A = 0.80∼0.91; $SSA_{M\text{-}A}$ = 0.05∼0.14 $\alpha_{\omega_0}A$ = 0.08∼0.17; $\alpha_{\omega_0\ M\text{-}A}$ = −0.16∼−0.10 MISR AOD spherical fraction = 0.8∼1.0	BB- dominated	SSA spectral dependence in MISR component particle models is not sufficiently steep
2	W. Africa–Jan, Feb, Mar (4) (total = 4 cases)	AOD_A = 0.5∼0.9; $AOD_{M\text{-}A}$ = −0.3∼−0.1 $\mathring{A}_A$ = 0.2∼0.8; $\mathring{A}_{M\text{-}A}$ = −0.1∼+0.9 SSA_A = 0.82∼0.92; $SSA_{M\text{-}A}$ = 0.08∼0.13 $\alpha_{\omega_0}A$ = −0.11∼−0.01; $\alpha_{\omega_0}M\text{-}A$ = 0.06∼0.09 MISR AOD spherical fraction = 0.8∼1.0	BB-dust mixed	no BB-dust mixtures in MISR mixture climatology
3	W. Africa–Dec, Jan, Mar, Jun (9) (total = 9 cases)	AOD_A = 0.2∼0.6; $AOD_{M\text{-}A}$ = −0.1∼+0.1 $\mathring{A}_A$ = 0.1∼0.8; $\mathring{A}_{M\text{-}A}$ = 0.1∼0.5 SSA_A = 0.93∼0.99; $SSA_{M\text{-}A}$ = 0.01∼0.05 $\alpha_{\omega_0}A$ = −0.08∼−0.01; $\alpha_{\omega_0}M\text{-}A$ = −0.02∼+0.07 MISR AOD spherical fraction = 0.4∼1.0	BB-dust mixed	no BB-dust mixtures in MISR mixture climatology
4	W. Africa–Dec, Feb (4) (total = 4 cases)	AOD_A = 0.9∼1.7; $AOD_{M\text{-}A}$ = −1.0∼−0.2 $\mathring{A}_A$ = 0.2∼0.4; $\mathring{A}_{M\text{-}A}$ = 0∼+0.5 SSA_A = 0.93∼0.96; $SSA_{M\text{-}A}$ = 0.04∼0.06 $\alpha_{\omega_0}A$ = −0.08∼−0.07; $\alpha_{\omega_0}M\text{-}A$ = 0.02∼0.07 MISR AOD spherical fraction = 0.5∼1.0	BB-dust mixed	poor separation of surface and aerosol properties in the MISR retrieval

origins suggest that cases in Group 1 are likely dominated solely by BB particles, whereas cases in other groups probably contain mixtures of BB with various fractions of weakly absorbing, medium to coarse size ($r_{pg,N}$ around 0.5 to 1 μm) dust particles. For each group, the unique patterns of AOD and/or SSA discrepancies, and the likely reasons for these discrepancies, are discussed subsequently.

2.2.1. Case Group 1 — BB Dominated

[14] For Group 1, MISR underestimates AOD by a small but systematic amount ($AOD_{M\text{-}A}$ = −0.17–0), and in most cases, substantially overestimates SSA ($SSA_{M\text{-}A}$ = 0.05–0.14), compared to AERONET (Figure 1d). In conditions when $\mathring{A}_A$ > 1.8, low biases in Ångstrom Exponent occur ($\mathring{A}_{M\text{-}A}$ = −0.6 and +0.2, Figure 1g). SSA spectral slope is also underestimated by around 0.1 in several cases in this group (Figure 1h).

[15] We expect that the underestimation of MISR v17 AOD and Ångstrom Exponent results from higher SSA and weaker SSA spectral slope retrieved by the Standard Algorithm. When the MISR retrieval algorithm overestimates SSA, the retrieved AOD tends to be lower than it would otherwise be, in order to compensate for the larger amount of scattering contributed by the particles to the observed TOA radiance [*Kahn et al.*, 2005a]. The retrieved SSA spectral dependence influences not only the retrieved mid-visible SSA (and therefore the AOD), but also the spectral dependence of AOD (i.e., Ångstrom Exponent). Large, positive α_{ω_0} is typically seen in absorbing BB particles in most field measurements, as discussed later in section 3. In the MISR v17 Standard Aerosol Retrieval Algorithm, the spherical absorbing particle components in the assumed particle climatology do cover the observed range of mid-visible SSA from 0.80 to 0.90, however, none of these components has a sufficiently steep, positive α_{ω_0} to match those measured in the field. These factors likely explain the abovementioned discrepancies.

[16] Note that, although the discrepancy in retrieved particle size can also produce Ångstrom Exponent biases, the number-weighted fine mode geometric mean radius in the MISR v17 retrievals (around 0.06 μm for all cases in group 1) agrees reasonably well with the fine mode size in the corresponding AERONET inversions (0.06–0.10 μm), so a discrepancy in size retrieval is less likely the reason for the AOD deviation of this group.

2.2.2. Case Group 2 — BB-Dust Mixed, 0.6 < AOD < 0.9

[17] Group 2 has moderately high AOD_A (0.5–0.9), Ångstrom Exponent between 0.2 and 0.8, absorbing SSA_A (0.82–0.92), and flat to moderately negative SSA spectral dependence ($\alpha_{\omega_{0A}}$ = −0.11 to −0.01), and likely contains mixtures of BB particles with some dust (Figure 1 and Table 2). Similar to cases of Group 1, MISR v17 also systematically underestimates AOD ($AOD_{M\text{-}A}$ = −0.3 to −0.1) in Group 2. MISR overestimates SSA ($SSA_{M\text{-}A}$ ∼ 0.1), Ångstrom Exponent ($\mathring{A}_{M\text{-}A}$ = −0.1 to +0.9), and SSA spectral slope ($\alpha_{\omega_{0M\text{-}A}}$ = 0.06 to 0.09) for this group.

[18] Dust particles generally exhibit an SSA spectral dependence (i.e., $\alpha_{\omega_0} < 0$) opposite to those of BB particles. Examples of dust particle optical models assumed in MISR v17 Aerosol Retrieval Algorithm can be found in Table 8. Dust models SSAs increase with increasing wavelength, but are steeper at shorter wavelengths and flatter at longer wavelengths than the relationship in equation (2). When the atmosphere contains both BB and dust particles, the positive and negative SSA wavelength dependences partly cancel with each other, and as a result, SSA of the entire mixture exhibits a flatter spectral slope.

[19] However, the assumed mixture climatology in the MISR v17 Aerosol Retrieval Algorithm does not have the combinations of absorbing spherical particles with dust particles likely to be present in these cases. The Standard Retrievals pick mixtures consisting of dust plus non-absorbing spherical particles, which result in an overestimation in mid-visible SSA and SSA spectral dependence, and therefore the retrievals are biased low in AOD and high in Ångstrom Exponent.

2.2.3. Case Group 3 — BB-Dust Mixed, AOD < 0.6

[20] Group 3 has $AOD_A < 0.6$, Ångstrom Exponent < 1, weakly absorbing SSA ($SSA_A = 0.93-0.99$), flat to moderately negative SSA spectral dependences ($\alpha_{\omega_{0A}} = -0.08$ to -0.01), and higher dust fractions (fraction spherical is as low as 0.4; Table 2) than Group 2. Unlike the systematic AOD low bias in Group 2, differences in mid-visible AOD are constrained to within ±0.1 with unbiased distribution. There is also a small positive bias in MISR mid-visible SSA ($SSA_{M\text{-}A} = 0-0.05$), SSA spectral dependence ($\alpha_{\omega_{0M\text{-}A}} = -0.02$ to $+0.07$), and Ångstrom Exponent ($\AA_{M\text{-}A} = 0.1-0.5$) for Group 3. As discussed earlier, these discrepancies are likely related to the limited selections BB-dust mixtures in the climatology of MISR Standard Aerosol Retrieval Algorithm. Because of the higher fractional contribution of dust to total AOD, the biases are less significant than those seen in group 2.

2.2.4. Case Group 4 — BB-Dust Mixed, AOD > 0.9

[21] Group 4 has significantly higher AOD ($AOD_A = 0.9-1.7$), small Ångstrom Exponent ($\AA_A = 0.2-0.4$), weakly absorbing SSA ($SSA_A = 0.93-0.96$), and moderately negative SSA spectral dependence ($\alpha_{\omega_{0A}} \sim -0.08$). Overall, the mixture properties are very similar to those derived for Group 3, but with substantially higher AOD. MISR significantly underestimates the mid-visible AOD ($AOD_{M\text{-}A} = -1.0$ to -0.2) and slightly overestimates the SSA spectral slope ($\alpha_{\omega_{0M\text{-}A}} = 0.02-0.07$) despite the small difference in SSA ($SSA_{M\text{-}A} \sim 0.05$). Ångstrom Exponent is also overestimated by as much as 0.5.

[22] The underestimation in AOD for this group probably results from factors other than the SSA and SSA spectral slope options available in aerosol climatology of the MISR v17 Algorithm. A major challenge in aerosol retrieval over land is that one cannot assume a dark surface, as is often true in the red and near-infrared bands over deep water, and as we adopt in the theoretical study (section 4) to simulate good viewing conditions. Aerosol properties retrieved from space can be very sensitive to surface condition. MISR provides simultaneous retrievals of atmospheric aerosols and the three-parameter, semi-empirical Rahman-Pinty-Verstraete (RPV) bidirectional reflectance distribution function (BRDF) surface model [*Rahman et al.*, 1993] at nine camera angles and four wavelengths [*Martonchik et al.*, 1998, 2002]; the first parameter characterizes the intensity of the surface reflectance, the second parameter indicates the level of symmetric surface anisotropy (the degree of "bowl" or "bell" shape), and the third represents the relative amount of forward and backward scattering from the surface. Under less hazy atmospheric conditions, the atmospheric contribution to the satellite signal is proportionately lower, and MISR surface property retrievals are expected to be more reliable.

[23] To assess the surface contribution to the top-of-atmosphere signal, we examine MISR surface parameters retrieved at the study locations, for the same viewing geometry, on less hazy days within a few weeks before or after each MISR-AERONET coincident event, and compare them with the values retrieved for the hazy days. In three of the four cases of group 4, the MISR Standard Algorithm retrieves much higher surface reflectance under hazy conditions; the first parameter in the RPV BRDF model is up to five times higher. (The fourth case has no successful surface retrieval on the hazy day owing to cloud contamination.) Since the surface itself probably did not change this dramatically between the clear and the hazy day, we conclude that poor separation of surface and atmospheric signals by the retrieval algorithm is likely to contribute significantly to the AOD underestimation seen in these very hazy cases.

[24] The analyses in this section, as summarized in Table 2, provide important suggestion for refining MISR retrievals for BB and dust-BB mixed cases. For BB-dominated cases, MISR v17 overestimates mid-visible SSA and underestimates mid-visible AOD, Ångstrom Exponent, and SSA spectral dependence. To eliminate these discrepancies, absorbing, spherical particle components with optical and microphysical properties matching BB smoke values observed in the field should be included in the retrieval algorithm particle climatology. For BB-dust mixed cases with moderate aerosol loadings, MISR v17 overestimates SSA, Ångstrom Exponent, and SSA spectral slope and underestimates AOD, suggesting that mixtures of absorbing, spherical BB particles with dust models should be added to the mixture selection in the algorithm. In addition, the algorithm's ability to separate surface from atmospheric contributions for extremely hazy conditions (mid-visible AOD > 0.8) needs to be refined.

3. BB Particle Property Characterization

[25] In the previous section, we referenced BB particle microphysical properties obtained from better-constrained sub-orbital observations, for use in the satellite retrieval algorithm. The purpose of this brief section is to identify likely natural ranges of BB particle size, SSA, and refractive index, from data reported in the published literature.

[26] *Reid et al.* [2004a, 2004b] give a comprehensive review of BB particle occurrence, properties, and evolution, and *Bond and Bergstrom* [2006] summarize the measured optical properties of light-absorbing carbon. Readers who wish to understand the current knowledge of gas-phase and particle-phase chemistry, associated particle microphysical and optical properties, and the issues related to comparing measurements among different instruments and inversion techniques should refer to these publications. Table 3 lists references providing ambient BB aerosol size and optical properties. Most of the data sources are field campaigns in major biomass burning areas, obtained since the late 1980s, such as SCAR-B (Smoke, Clouds, and Radiation-Brazil) and SAFARI (Southern African Regional Science Initiative) 2000. Another important data source is the continuous ground-based observation from AERONET.

[27] Although we seek to understand how BB physical properties vary with region, smoke age, vegetation type, and combustion phase, it is difficult to identify specific trends when comparing measurements made with different in situ instruments and retrieval techniques. Data collected from the literature are summarized in Table 4, showing the averages and ranges of reported values. On the basis of the plume age information reported in the literature, for timescales relevant to satellite measurements, we categorize data collected from plumes less than one day old as fresh smoke, whereas plumes one to three days old as aged smoke. If the plume is older than three days, or if plume

Table 3. BB Aerosol Physical and Optical Property References Covered in This Review of the Field Experiment Literature

Region	Field Experiment	Experimental Period	Vegetation	Reference for Parameter[d]		
				Size[a]	SSA[b]	n_r-in_i[c]
S. Africa	SAFARI-92	Aug–Oct 1992	savanna	1		
	SAFARI 2000	Aug–Sep 2000	savanna	2	3	4
	SAFARI 2001	Aug–Sep 2001	savanna		5	
	AERONET	1995–2000	savanna	6	6	6
Amazon Basin	BASE-A	Sep 1989	cerrado	7		
	LBA-EUSTACH	1999	forest	8	8	8
	TRACE A	Sep–Oct 1992	forest	9	9	
	SCAR-B	Aug–Sep 1995	forest/cerrado	10	11	12
	AERONET	1993–1994; 1998–1999; 2002	forest	6	6	6
	AERONET	1993–1995	cerrado	13	13	13
N. America	indept. study	Sep 1986–Sep 1989	boreal forest	14	15	
	ARM SGP	1997–2001	N/A		16	
	AERONET	1994–1998; 2002	boreal forest	6	6	6
(California)	indept. study	Dec 1986; Jun 1987	chaparral		15	
(Pacific N. W.)	SCAR-C	Sep 1994	boreal forest	17	17	18
(Canada)	BOREAS	Jul–Aug 1994	boreal forest		19	
Central America	indept. study	May 1998	N/A	20	21	20

[a]Size distribution parameters.
[b]Single scattering albedo.
[c]Refractive index.
[d]Reference: 1. *Le Canut et al.* [1996a, 1996b]. 2. *Eck et al.* [2003b]; *Haywood et al.* [2003b]; *Pósfai et al.* [2003]. 3. *Abel et al.* [2003]; *Bergstrom et al.* [2003]; *Eck et al.* [2003b]; *Formenti et al.* [2003]; *Haywood et al.* [2003a, 2003b]; *Pilewskie et al.* [2003]. 4. *Haywood et al.* [2003a, 2003b]. 5. *Magi et al.* [2003]. 6. *Dubovik et al.* [2002]; *Eck et al.* [2003a]. 7. *Holben et al.* [1991]. 8. *Guyon et al.* [2003]. 9. *Anderson et al.* [1996]. 10. *Reid and Hobbs* [1998]; *Reid et al.* [1998b]; *Reid et al.* [1999]; *Remer et al.* [1998]. 11. *Dubovik et al.* [1998]; *Eck et al.* [1998]; *Hobbs et al.* [1997]; *Martins et al.* [1998]; *Reid and Hobbs* [1998]; *Reid et al.* [1998a, 1998b]; *Reid et al.* [1999]; *Remer et al.* [1998]. 12. *Eck et al.* [1998]; *Yamasoe et al.* [1998]. 13. *Dubovik et al.* [2002]. 14. *Einfeld et al.* [1991]; *Radke et al.* [1991]. 15. *Radke et al.* [1988]; *Radke et al.* [1991]. 16. *Iziomon and Lohman* [2003]. 17. *Hobbs et al.* [1996]; *Martins et al.* [1996]; *Trentmann et al.* [2002]. 18. *Trentmann et al.* [2002]. 19. *Miller and O'Neill* [1997]. 20. *Kreidenweis et al.* [2001]. 21. *Kreidenweis et al.* [2001]; *Zhang et al.* [2001].

age is not reported, the data are categorized as regional haze. Therefore regional haze can cover the widest range of smoke ages, combustion efficiencies, and flame phases. Note that the averages in Table 4 are simply the means of all available measurements; they are not corrected for different instrument and sampling biases, and can only be considered as a general indication of the parameters in each plume category.

[28] BB aerosol size distributions are usually expressed in terms of normalized lognormal distributions,

$$\frac{dN(r_{p,N})}{d\ln r_{p,N}} = \frac{1}{(2\pi)^{1/2}\ln\sigma_g}\exp\left(-\frac{\left(\ln r_{p,N}-\ln r_{pg,N}\right)^2}{2\ln^2\sigma_g}\right), \quad (3)$$

where $dN(r_{p,N})$ the particle number concentration in a $d\ln r_{p,N}$ interval, $r_{pg,N}$ is the geometric mean radius, and σ_g is the geometric standard deviation. We summarize here only measurements for spherical, fine-mode ($r_{pg,N} < 1.0\ \mu$m) particles, which are dominated by carbonaceous particles generated by combustion processes. Figures 2a and 2b give the values of fine mode $r_{pg,N}$ and σ_g, assembled from the data sources in Table 3. The vertical lines display the mean values for fresh smoke, aged smoke, and regional haze (colored red, blue, and green, respectively), whereas the grey bars show the ranges of reported values. In general, $r_{pg,N}$ is about 0.05 μm larger and σ_g is 0.05–0.1 smaller for aged plumes than for fresh plumes, suggesting growth during aging, a fairly well-established phenomenon [e.g., *Reid et al.*, 2004a, 2004b]. The data for regional haze, which covers smokes of various ages, generally shows an average size between those of fresh and aged plumes, and a much larger range of σ_g. On a regional basis, $r_{pg,N}$ and σ_g for Amazon BB aerosol seem to be generally larger than those in Africa, whereas the aged plumes in North America

Table 4. Profiles of Fresh Plumes, Aged Plumes, and Haze Based on the Literature[a]

Smoke Type	$r_{pg,N}$, μm	σ_g	$\omega_{0,450}$	$\omega_{0,550}$	$\omega_{0,670}$	$\omega_{0,700}$	$\omega_{0,870}$	$n_{r,550}$
Fresh plume	0.03–0.17	1.30–1.91	0.77–0.86	0.70–0.94	0.60	0.67–0.80	N/A (N/A)	1.50–1.54
(<one day old)	(0.074)	(1.68)	(0.83)	(0.84)	(0.60)	(0.74)		(1.53)
	n = 13	n = 13	n = 6	n = 32	n = 1	n = 6	n = 0	n = 4
Aged plume	0.08–0.20	1.25–1.65	0.87–0.94	0.78–0.94	0.86–0.88	0.83–0.91	0.83–0.92	1.50–1.54
(1 to 3 days old)	(0.12)	(0.49)	(0.91)	(0.88)	(0.87)	(0.87)	(0.85)	(1.52)
	n = 10	n = 10	n = 17	n = 33	n = 6	n = 17	n = 8	n = 5
Regional haze	0.03–0.14	1.30–2.01	0.84–0.87	0.79–0.94	0.84–0.98	0.69–0.75	0.80–0.96	1.43–1.55
(>3 days old or	(0.07)	(1.67)	(0.86)	(0.85)	(0.92)	(0.72)	(0.86)	(1.50)
mixed age)	n = 24	n = 24	n = 3	n = 38	n = 9	n = 3	n = 12	n = 6

[a]The first row for each smoke type shows the range, second row, the average in parentheses, and third row, the number of reported values.

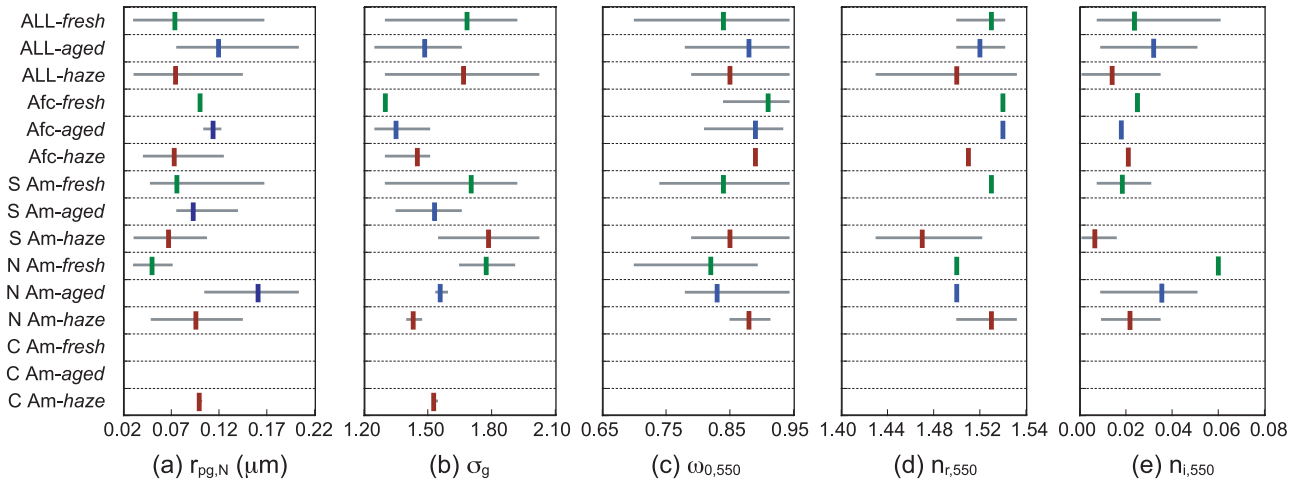

Figure 2. The means (vertical lines) and ranges (grey bars) of reported physical and optical parameter values for haze, aged, and fresh plumes in different regions: (a) number-weighted geometric mean radius ($r_{pg,N}$), (b) geometric standard deviation (σ_g), (c) single scattering albedo at 550 nm ($\omega_{0,550}$), (d) real part of refractive index (n_r) at 550 nm, and (e) imaginary part of refractive index (n_i) at 550 nm. The vertical lines are red for fresh plumes (<1 day old), blue for aged plumes (1–3 days old), and green for regional haze (>3 days old or mixed). (Abbreviations: Afc = Africa, S Am = South America, N Am = North America, C Am = Central America).

seem to exhibit the largest particle size. Besides fine-mode particles, in the literature reporting multimodal size measurements, small fractions of coarse-mode particles, with $r_{pg,N}$ around 1.0 to 1.5 μm, are also mentioned [e.g., *Haywood et al.*, 2003b; *Kreidenweis et al.*, 2001], mostly as soil re-suspended by pyro-cumulus thermal updrafts, ash-debris [*Reid and Hobbs*, 1998], and transported mineral dust. In the sensitivity study of section 4, we consider only the fine-mode particles. Coarse-mode particles will be considered in the Research Retrievals of section 5.

[29] Figure 2c shows the reported ranges of published SSA at $\lambda = 550$ nm ($\omega_{0,550}$). Fresh plumes generally exhibit the smallest mid-visible SSA ($\omega_{0,550}$ around 0.85). The increase of SSA with plume age is attributed to the growth of particles into a size range where scattering is a large proportion of total extinction [e.g., *Hobbs et al.*, 1997]. Some studies have shown that the southern African savanna smoke is the most absorbing [*Dubovik et al.*, 2002; *Eck et al.*, 2003a], presumably because biomass in the savanna ecosystem tends to be consumed by flaming combustion, which produces a higher fraction of black carbon (BC) than smoldering combustion.

[30] In addition, the wavelength dependence of SSA can also vary significantly (not shown in Figure 2). The spectral slope of SSA, as defined by α_{ω_0} in equation (2), is expected to be steeper (0.1–0.4) for BB particles having mid-visible SSA lower than around 0.85 [e.g., *Hobbs et al.*, 1997; *Reid and Hobbs*, 1998; *Eck et al.*, 2003b; *Haywood et al.*, 2003b], whereas α_{ω_0} is thought to be flatter (0.05–0.1) for particles having mid-visible SSA exceeding 0.85 [e.g., *Dubovik et al.*, 2002; *Eck et al.*, 2003b; *Haywood et al.*, 2003a, 2003b]. This expectation is difficult to confirm for lack of sufficient simultaneous, multichannel measurements.

[31] Also, most sources do not explicitly report the ambient relative humidity during measurement, and sometimes it is not clear whether wet or dry particles were measured. In fact, changes in hygroscopicity with chemical aging, and the effects of particle hygroscopic growth on particle optical properties are the most uncertain properties for BB aerosols [*Reid et al.*, 2004b; *Petters et al.*, 2006]. As a result, it is difficult to correct the reported data for hygroscopic growth. Instead, we study a parameter space that covers the range of sizes and SSA likely to include BB particles under most natural conditions (see section 4).

[32] Refractive index ($n_r - in_i$) governs particle scattering and absorption. The real (n_r) and imaginary (n_i) parts are both functions of wavelength. Figures 2d and 2e show published n_r and n_i values, respectively, for BB aerosols at 550 nm. Some of these values were calculated assuming: (1) a given mixing rule, such as BC core with organic carbon (OC) shell, or homogeneous mixing, (2) average mass or volume fraction of BC in the particle, and (3) aerosol density, using experimental values of refractive indices for pure substances ($1.75-0.44i$ at 550 nm for BC; $n_r = 1.52$ to 1.54 and $n_i = 0$ to 0.0035 for OC at all wavelengths) [e.g., *Haywood et al.*, 2003b; *Trentmann et al.*, 2002]. Other data were taken from inversions of radiometric measurements [e.g., *Yamasoe et al.*, 1998]. Although $n_{r,550}$ for regional haze covers the range of 1.44 to1.55, its value is generally smaller than that of younger aerosols. As expected from the observed increase in SSA as smoke ages, fresh smoke has a higher n_i value, especially in North America ($n_{i,550} \sim 0.06$).

4. Theoretical Sensitivity Study for BB Aerosol Components

[33] As discussed in section 3, the size and optical properties of BB particles can vary tremendously with ambient conditions. To understand the precision with which we can expect MISR to distinguish among BB particles of

Table 5. BB Aerosol Component Models[a]

#	Component Model	$r_{pg,N}$, μm	σ_g	$\omega_{0,446}$	$\omega_{0,558}$	$\omega_{0,672}$	$\omega_{0,867}$	n_r (all λ's)	Description
1	VS_VA	0.04	1.6	0.782	0.737	0.691	0.613	1.50	very small, very absorbing
2	S_VA	0.07	1.6	0.782	0.737	0.691	0.613	1.50	small, very absorbing
3	M_VA	0.13	1.6	0.782	0.737	0.691	0.613	1.50	medium, very absorbing
4	L_VA	0.16	1.6	0.782	0.737	0.691	0.613	1.50	large, very absorbing
5	VS_A	0.04	1.6	0.861	0.838	0.816	0.777	1.50	very small, absorbing
6	S_A	0.07	1.6	0.861	0.838	0.816	0.777	1.50	small, absorbing
7	M_A	0.13	1.6	0.861	0.838	0.816	0.777	1.50	medium, absorbing
8	L_A	0.16	1.6	0.861	0.838	0.816	0.777	1.50	large, absorbing
9	VS_LA	0.04	1.6	0.910	0.899	0.888	0.868	1.50	very small, less absorbing
10	S_LA	0.07	1.6	0.910	0.899	0.888	0.868	1.50	small, less absorbing
11	M_LA	0.13	1.6	0.910	0.899	0.888	0.868	1.50	medium, less absorbing
12	L_LA	0.16	1.6	0.910	0.899	0.888	0.868	1.50	large, less absorbing
13	VS_WA	0.04	1.6	0.950	0.939	0.928	0.908	1.50	very small, weakly absorbing
14	S_WA	0.07	1.6	0.950	0.939	0.928	0.908	1.50	small, weakly absorbing
15	M_WA	0.13	1.6	0.950	0.939	0.928	0.908	1.50	medium, weakly absorbing
16	L_WA	0.16	1.6	0.950	0.939	0.928	0.908	1.50	large, weakly absorbing

[a]Size distribution lower and upper cut-off sizes are 0.005 and 1.5 μm, respectively.

different sizes and optical properties, over the range of natural variation, we perform a theoretical sensitivity study before proposing specific updates to the representative BB particle models in the Standard Algorithm.

[34] The theoretical study aims at answering two important questions. (1) If the atmospheric aerosol is dominated spherical particles having a given size distribution and SSA within the natural BB particle range, how precisely can the size and SSA be retrieved from TOA MISR radiances under good but not necessarily ideal conditions? (2) How does retrieval sensitivity to size and SSA vary when the atmospheric aerosol properties change? In addition to indicating which spherical components should be included in the Standard Aerosol Retrieval Algorithm to represent BB particles, the theoretical study conclusions will help in interpreting results of actual retrievals for BB cases, as we do in section 5.

[35] Our approach follows *Kahn et al.* [2001]. We set up the Research Aerosol Retrieval algorithm with simulated TOA reflectances for a range of aerosol mixtures and optical depths, to serve as the "comparison space." For each test, we select one component and AOD, as the "atmosphere." The simulated reflectances for this component are treated as measurements in the retrieval process. The retrieved range of AODs and particle types is then compared to the "atmosphere," to establish the sensitivity of the retrieval method. In this case, we focus the study on the two-dimensional particle property space of size and SSA for spherical particles, representing the natural range of BB components.

4.1. BB Aerosol Components and Mixing Groups

[36] A set of 16 spherical aerosol components is developed for the sensitivity study radiance simulations (Table 5) that captures the observed range of natural BB particle properties based on Table 4. Each aerosol component is defined by a fixed composition and unimodal, lognormal size distribution. They span sizes from very small ($r_{pg,N}$ = 0.04 μm) to large ($r_{pg,N}$ = 0.16 μm) and mid-visible SSA values from very absorbing ($\omega_{0,558}$ = 0.74) to weakly absorbing ($\omega_{0,558}$ = 0.94). As discussed earlier, the wavelength dependence of SSA, α_{ω_0}, may also vary with particle type. Here we do not control for this parameter explicitly; rather, we chose α_{ω_0} = 0.37 for very absorbing particles [e.g., *Hobbs et al.*, 1997; *Reid and Hobbs*, 1998], 0.15 for absorbing particles, and 0.07 for less and weakly absorbing ones.

[37] We create a range of mixtures, to be used as the comparison space in the Research Retrieval algorithm, by defining eight "mixing groups" (Table 6). Each mixing group is a set of external, four-component aerosol mixtures, with the proportion of each component allowed to vary from 0 to 100 percent, following *Kahn et al.* [2001]. The components are selected from the 16 given in Table 5. Mixing groups 1 to 4 aim at exploring sensitivity to particle size by choosing components having similar mid-visible SSA values but different radii (Table 6). Mixing groups 5 to 8, containing components having similar radii but different SSAs, are intended to test MISR's sensitivity to SSA.

Table 6. BB Aerosol Mixing Groups[a,b]

Mixing Group (Description)	Component 1	Component 2	Component 3	Component 4
M1 (SSA = VA; size = VS-L)	1_VS_VA	2_S_VA	3_M_VA	4_L_VA
M2 (SSA = A; size = VS-L)	5_VS_A	6_S_A	7_M_A	8_L_A
M3 (SSA = LA; size = VS-L)	9_VS_LA	10_S_LA	11_M_LA	12_L_LA
M4 (SSA = WA; size = VS-L)	13_VS_WA	14_S_WA	15_M_WA	16_L_WA
M5 (SSA = VA-WA; size = VS)	1_VS_VA	5_VS_A	9_VS_LA	13_VS_W
M6 (SSA = VA-WA; size = S)	2_S_VA	6_S_A	10_S_LA	14_S_WA
M7 (SSA = VA-WA; size = M)	3_M_VA	7_M_A	11_M_LA	15_M_WA
M8 (SSA = VA-WA; size = L)	4_L_VA	8_L_A	12_L_LA	16_L_WA

[a]Target atmospheric components chosen to model BB particles in the theoretical sensitivity study, of which the AOD is set to 0.2 or 0.5, are 1_VS_VA, 3_M_VA, 4_L_VA, 6_S_A, 7_M_A, 8_L_A, 11_M_LA, and 16_L_WA.

[b]VS = very small, S = small, M = medium, and L = large; VA = very absorbing, A = absorbing, LA = less absorbing, and WA = weakly absorbing.

4.2. Radiative Transfer Simulations, and the χ^2 Test Variables for Evaluating Agreement Between Simulated Reflectances in the Sensitivity Test

[38] Sensitivity calculations were carried out for sixteen atmospheres, each assumed to contain 100 percent of one of eight component particles selected to span the size-SSA space (as listed in footnote (a) in Table 6), and with total column AOD of 0.2 or 0.5. The TOA equivalent reflectances are simulated by the radiative transfer (RT) code developed by the MISR team [*Martonchik et al.*, 1998] based on the matrix operator method [*Grant and Hunt*, 1968]. Following the assumptions adopted in previous theoretical calculations [e.g., *Kahn et al.*, 1997, 2001; *Kalashnikova and Kahn*, 2006], a cloud-free, Rayleigh scattering atmosphere over a Fresnel-reflecting dark water surface, with 1 atm surface pressure, 2.5 ms^{-1} wind speed, and a standard midlatitude lapse rate profile is assumed. The aerosols are assumed to be concentrated in a single near-surface layer, and the influence of their vertical distribution is neglected for these tests. These assumptions are designed to simulate good but not ideal viewing conditions, with the understanding that as actual conditions degrade, so will the sensitivity of the MISR retrievals. The TOA radiance for all MISR view angles and wavelengths is derived. The ratio of the radiances multiplied by π to the exo-atmospheric solar irradiance then gives the equivalent reflectances.

[39] The same radiative transfer code and assumptions about surface and atmospheric condition are also applied to calculate the equivalent reflectances of the entire comparison space of eight mixing groups listed in Table 6. Mixtures composed of all possible combinations of the four components in a mixing group are considered, with the AOD fraction of each component allowed to vary from 0 to 100 percent in 5 percent increments. Comparison space reflectances are calculated also as a function of total column AOD from 0 to 1, in intervals of 0.05.

[40] Theoretical retrievals are then performed for the 16 atmospheres. The algorithm assesses how closely the reflectances produced for all the mixtures and AODs in the comparison space match those of the atmosphere, based on the χ^2 statistical formalism described in detail by *Kahn et al.* [1997, 1998, 2001]. Briefly, χ^2_{abs}, χ^2_{geom}, and χ^2_{spec} compares absolute reflectances, reflectance ratios normalized to one view angle, and reflectance ratios normalized to one wavelength, respectively, between the atmosphere and the comparison space. Each test variable is normalized by the number of channels used. The reflectances of a four-component mixture are considered indistinguishable from those of the atmosphere if the maximum of the three χ^2 test variables,

$$\chi^2_{\max} = \mathrm{Max}\{\chi^2_{abs}, \chi^2_{geom}, \chi^2_{spec}\} \quad (4)$$

is less than a chosen constraint. $\chi^2_{\max} < 1$ means the average difference between the atmosphere and a comparison model is less than the associated measurement error. In this study the criterion for a comparison model to be considered a match is $\chi^2_{\max} < 1.5$. This choice aims at realistically characterizing MISR sensitivity to aerosol properties under natural, good, but not ideal observing conditions [*Kahn et al.*, 2001]. The smaller the range of comparison models, in particle size, SSA, and AOD, that produce acceptable matches to the atmosphere, the greater the measurement sensitivity.

4.3. Results of MISR Theoretical Sensitivity to BB Components

[41] Figures 3 and 4 display the sensitivity results for the eight atmosphere AOD = 0.2 and the eight atmosphere AOD = 0.5 cases, respectively. Each sub-panel of these figures is a plot, with particle size increasing along the horizontal axis and SSA decreasing up the vertical axis, presenting the range of comparison models that produce acceptable matches to a specific atmosphere component. The number designation of the atmosphere component for each panel is given in the upper-left corner. For reference, the panel in the lower left of each figure shows the locations of all 16 components used for the entire sensitivity study (Table 5) in this same size-SSA space.

[42] Green dots in each sub-panel locate the component particles tested against the corresponding atmosphere, and the circled areas around them are proportional to the retrieved AOD fractional contribution for the components. Larger circles indicate that a larger fraction of that component provided an acceptable match to the atmosphere in the retrieval results. (The gray circle in the lower left reference panel is a scale for the size of the 100 percent circle.) In each sub-panel, the circle of minimum retrieved fraction for the atmosphere component itself (the ''correct'' answer) is shaded red and that of the maximum fraction is blue. For components in the retrieval comparison space having different size and/or SSA, the circles are black if the maximum retrieved fraction is higher than about 20 percent; otherwise the circles are shaded gray. (The 20% value is selected for illustration, because component retrievals are apparently significant if they comprise more that about 20% of the total column AOD, based on pervious sensitivity analysis [*Kahn et al.*, 2001]).

[43] So, for example, in the top middle panel of Figure 3, for which the atmosphere is assumed to contain 100% of Particle #3, 80–100% of the total column AOD was assigned to Particle 3 by the retrieval algorithm from all mixtures and AODs tested; no mixtures containing more than 20% of any other component produced an acceptable match to the simulated TOA reflectances except a slightly larger particle having the same SSA (Particle #4). In contrast, for the middle sub-panel of this figure, showing the retrieval results when the atmosphere contains Particle #7, the solution space includes AOD fractions of this particle ranging from less than 0.2 up to 1.0, and mixtures containing significant fractions of particles having the same size but SSA ranging from 0.75 to 0.95 also provide acceptable matches to the simulated TOA reflectances. So in this case, there is poor sensitivity to SSA, but still relatively good sensitivity to particle size. Also note that the sub-panels are organized in the overall figure so that atmospheres containing more absorbing particles are at the top and those containing larger particles are to the right. This is indicated with labels at the bottom and the left sides of the figure, making it easy to identify the variations in size and SSA sensitivity by comparing adjacent sub-plots.

[44] For the parameter space of Figures 3 and 4, the sub-panels at the corners generally show the highest sensitivity,

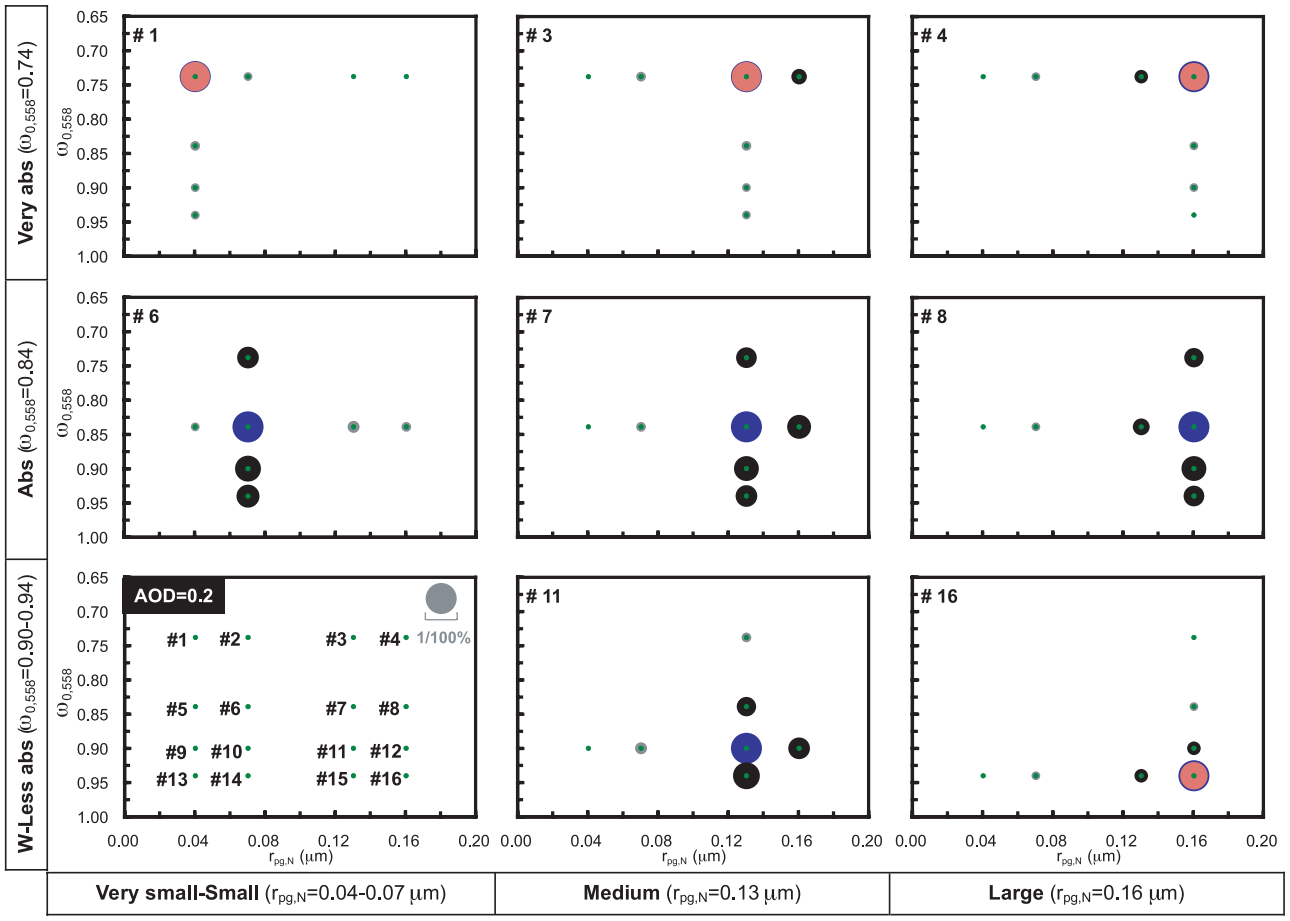

Figure 3. Sensitivity results of eight target atmospheric BB components assuming AOD = 0.2. Each individual sub-plot shows the results for comparisons against one target atmospheric component (marked at the upper-left corner of each sub-plot), with the comparison space $r_{pg,N}$ and $\omega_{0,558}$ values organized along the x and y axes, respectively. Overall, the plot array is arranged by the $r_{pg,N}$ and $\omega_{0,558}$ of the target atmospheric components (marked at the bottom and the left of the plate). The lower-left sub-plot shows positions of all components on the $r_{pg,N}$–$\omega_{0,558}$ plane (green spots). Retrieved component fractions are proportional to the area of colored circles; the gray circle in the lower-left plot is the scale of 100% fraction. For the target atmospheric component in each panel, the red circle shows the minimum retrieved fraction, and the blue shows the maximum fraction. For the other components, the circle shows only the maximum fraction, and is shaded black if more than 20%, otherwise, gray. Conditions of 1 atm surface pressure and 2.5 ms^{-1} wind speed, for midlatitude geometry, over a dark water surface, are assumed in these radiative transfer calculations.

indicated by the very large red circles and fewer (or no) small black circles. So MISR can accurately retrieve particles at the extremes of SSA (either very absorbing or weakly absorbing) and size (either small or large). Sub-panels in the top row of Figure 3 demonstrate that SSA can be accurately retrieved when the atmosphere contains very absorbing particles ($\omega_{0,558} \sim 0.74$) for any size category, even for total column AOD of 0.2. However, sub-panels in the second row show that MISR has poor sensitivity to SSA when the atmospheric components are absorbing ($\omega_{0,558} \sim 0.84$); the retrieved SSA spans very absorbing to weakly absorbing for particles of all sizes (black circles in the vertical direction), and the sensitivity does not improve when the atmospheric AOD is raised to 0.5 (Figure 4).

[45] For size discrimination, sub-panels in the left columns of Figures 3 and 4 show that the sizes of very small to small size ($r_{pg,N}$ = 0.04–0.07 μm) can be successfully retrieved in all SSA categories in both the AOD = 0.2 and 0.5 cases. Sub-panels in the right columns show that the size of large particles ($r_{pg,N} \sim 0.16$ μm) can be accurately retrieved only when AOD = 0.5. On the other hand, sub-panels in the middle column show that atmospheric components of medium size ($r_{pg,N} \sim 0.13$ μm) can be separated from components of small size but not from those of large size, especially for absorbing to weakly absorbing particles; size sensitivity to medium-large particle improves somewhat when AOD is increased to 0.5.

[46] In the theoretical calculations, retrieved total column AOD is constrained to at least ±0.05 in all cases. The overall

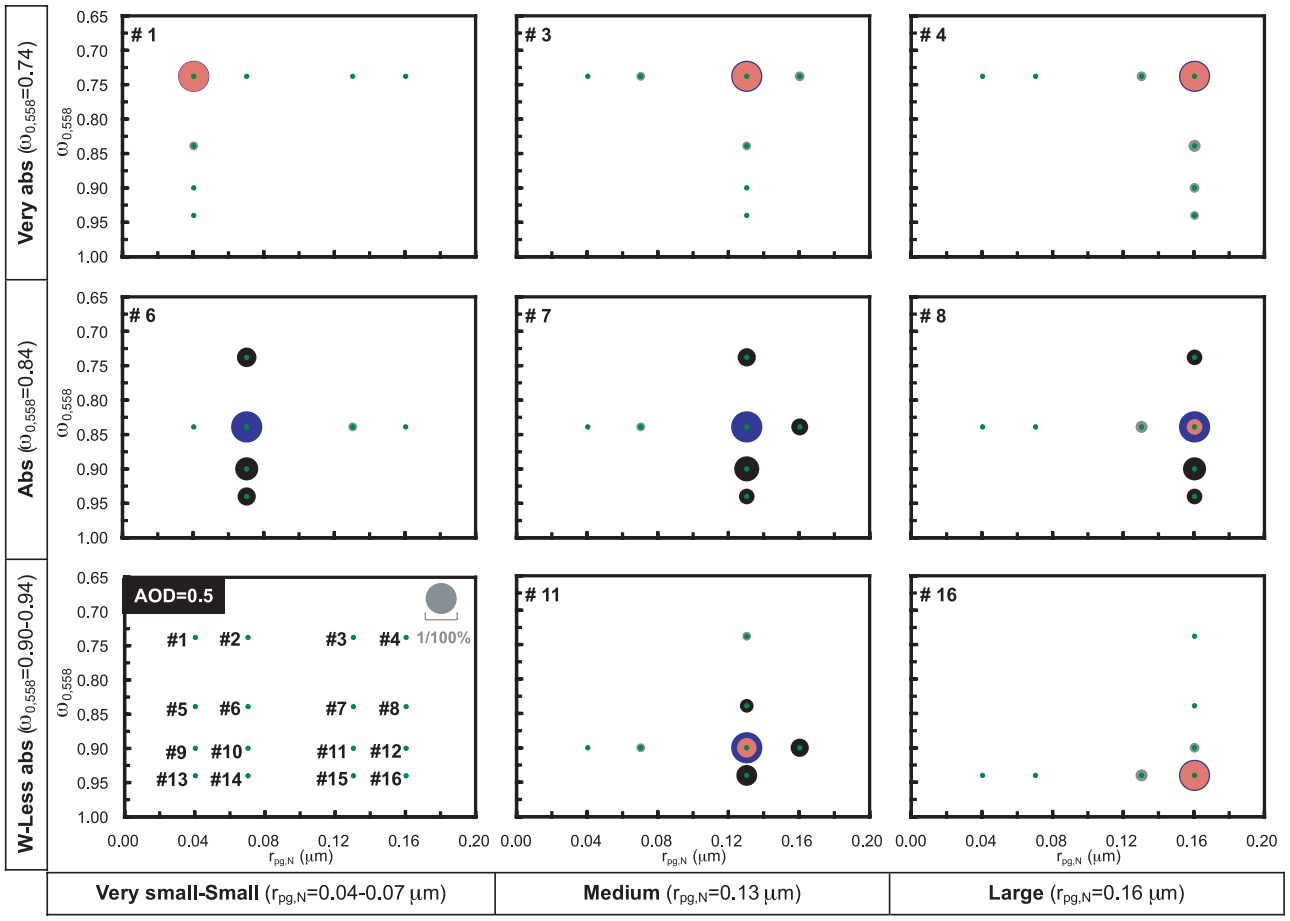

Figure 4. Same as Figure 3, but for atmospheric BB components with having AOD = 0.5.

sensitivity results are summarized in Table 7, which captures components contributing 20 percent or more to the total mid-visible AOD. Generally, in the parameter space covered by representative BB aerosol types, it is possible for MISR to identify two to three size categories. Two to three SSA categories can be identified when the atmospheric particles are very absorbing, or are less to weakly absorbing, but sensitivity to SSA is poor for absorbing particles ($\omega_{0,558} \sim 0.84$). *Kahn et al.* [2001] showed that, under good viewing conditions, MISR can distinguish three to five size bins with an uncertainty of about 20 percent in particle component mid-visible AOD; also among spherical components, MISR can distinguish two to four groups in SSA. The results in this study are consistent with, and add considerable detail to the conclusions by *Kahn et al.* [2001].

[47] We also performed a similar sensitivity analysis for non-absorbing particles ($\omega_0 = 1.0$ for all wavelength) in the above four size categories, though they are not shown in Figures 3 and 4 to reduce clutter. The results indicate that MISR can successfully separate non-absorbing particles (e.g., sulfates) from BB components of similar sizes, even for a total column AOD of 0.2. In addition, the theoretical sensitivity of MISR to particle sphericity was investigated by *Kahn et al.* [1997] and *Kalashnikova and Kahn* [2006], so it is not repeated here. These studies conclude that over calm ocean surface, MISR can distinguish non-spherical, absorbing particles (e.g., mineral dust) from spherical, absorbing particles over the natural range of particle sizes and AOD > 0.05, and the optical depth itself is retrieved to the accuracy of at least 0.05 or 10%.

5. MISR Research Retrieval Study of Field Cases With Proposed BB Components and Detailed Surface Characterization

[48] In this section we perform detailed Research Retrieval analysis on four near-coincident MISR-AERONET cases from section 2, one from each case group. The objective is to assess the impact of adding BB component models and possibly improving surface characterization on MISR Standard aerosol retrieval results, by comparing the Research with the MISR v17 Standard Retrievals. We also examine the uncertainties introduced by spatial variability, by analyzing multiple patches in the vicinity of the AERONET surface station for each case. The MISR Research Aerosol Retrieval Algorithm is similar to the Standard Algorithm, which uses observed MISR TOA radiances but surface properties obtained under clean air conditions (section 5.1). The major differences between the Research and the Standard algorithms of relevance here are (1) the Research algorithm allows four components in the mixture climatology, whereas the Standard Retrievals allows three, (2) the surface properties in the Research Retrievals can be prescribed, whereas the Standard Retrievals automatically use the RPV bidirectional surface model retrieved simultaneously by MISR, and (3) pixel patches of arbitrary size and location can be analyzed

Table 7. Summary of Sensitivity Results for Unimodal BB Particle Cases[a]

	Size Discrimination			
	Retrieved AOD and Particle Size (for Assumed Atmospheric AOD = 0.2)		Retrieved AOD and Particle Size (for Assumed Atmospheric AOD = 0.5)	
Atmospheric Component	AOD	Size	AOD	Size
SSA = Very absorbing				
Very small (1_VS_VA)	0.20	very small	0.50	very small
Medium (3_M_VA)	0.20	medium to large	0.50	medium
Large (4_L_VA)	0.20	medium to large	0.45–0.50	large
SSA=Absorbing				
Small (6_S_A)	0.20	small	0.50	small
Medium (7_M_A)	0.20	medium to large	0.50	medium to large
Large (8_L_A)	0.20	medium to large	0.50	large
SSA = Weakly less absorbing				
Medium (11_M_LA)	0.20	medium to large	0.50	medium to large
Large (16_L_WA)	0.20	medium to large	0.50	large
	SSA Discrimination			
	Retrieved AOD and Particle SSA[a] (Assumed AOD = 0.2)		Retrieved AOD and Particles SSA[a] (Assumed AOD = 0.5)	
Atmospheric Component	AOD	SSA	AOD	SSA
Size = Very small-small				
Very absorbing (1_VS_VA)	0.20	very absorbing	0.50	very absorbing
Absorbing (6_S_A)	0.20	very to weakly absorbing	0.50	very to weakly absorbing.
Size = Medium				
Very absorbing (3_M_VA)	0.20	very absorbing	0.50	very absorbing
Absorbing (7_M_A)	0.20	very to weakly absorbing	0.50	very to weakly absorbing
Less Absorbing (11_M_LA)	0.20	absorbing to weakly absorbing	0.50	absorbing to weakly absorbing
Size = Large				
Very absorbing (4_L_VA)	0.20	very absorbing	0.45–0.50	very absorbing
Absorbing (8_L_A)	0.20	very to weakly absorbing	0.50	very to weakly absorbing
Weakly abs. (16_L_WA)	0.20	less to weakly absorbing	0.50	Weakly absorbing

[a]Retrieved Particles refer to the components that contribute over 20% to the total aerosol optical depth, for retrieval results obtained with $\chi^2_{max} < 1.5$.

with the Research algorithm, whereas the Standard algorithm operates automatically on a fixed grid of 16 by 16 pixel patches.

[49] In addition to the 16 BB component models (Table 5), two representative dust particle models [*Kalashnikova et al.*, 2005], one accumulation mode sulfate model, and two coarse mode sea salt models were included in the particle climatology of the Research Retrieval Algorithm for this study; their properties are given in Table 8. Along with the 8 mixing groups in Table 6, 37 additional mixing groups (not shown) of BB components with dust, sulfate, and sea salt were added to the comparison space, to account for realistic field conditions.

5.1. Patches and Surface Characterization for Selected Field Cases

[50] Cuiaba-Miranda on 31 August 2001 (Cuiaba-Miranda_20010831), Ilorin on 24 February 2001 (Ilorin_20010224), Ouagadougou on 18 December 2000 (Ouagadougou_20001218), and Ilorin on 17 February 2001 (Ilorin_20010217) were chosen to represent the four groups discussed in section 2. For each case, MISR Research Retrievals were performed on four to seven 3 by 3 pixel patches. One patch was chosen at the exact location of the AERONET site (patch P0). The other patches were chosen at locations close to the AERONET sites where dark and homogenous surface is present in the MISR image. (The homogeneity criterion used requires the variance of the band-corrected equivalent reflectance for the clean-day orbit to be <10% of the mean.) Table 9 lists the MISR overpass orbits and patch locations for the four selected cases. Multiple patches are chosen for each case because the surface conditions around the AERONET site may be variable. Comparisons among various darkest patches reveal the impact of scene spatial variability.

[51] As mentioned in section 2, successful aerosol retrievals depend heavily on having accurate surface characterization.

Table 8. Additional Components Used in the MISR Research Aerosol Retrieval Algorithm for the Four Representative Coincident BB Cases

Component Model	$r_{pg,N}$, μm[a]	σ_g	$\omega_{0,446}$	$\omega_{0,558}$	$\omega_{0,672}$	$\omega_{0,867}$	n_r (all λ's)	Description
Medium dust	0.50	1.5	0.919	0.977	0.994	0.997	1.51	weakly absorbing grains[b]
Coarse dust	1.00	2.0	0.810	0.902	0.971	0.983	1.51	weakly absorbing spheroids[b]
Sulfate	0.06	1.7	1.000	1.000	1.000	1.000	1.45	small, non-absorbing sphere[c]
Medium sea salt	0.50	1.85	1.000	1.000	1.000	1.000	1.45	medium, non-absorbing sphere[c]
Coarse sea salt	1.00	1.9	1.000	1.000	1.000	1.000	1.45	large, non-absorbing sphere[c]

[a]Size distribution lower and upper cut-offs are 0.1 and 1.0 μm for medium dust, 0.1 and 6.0 μm for coarse dust, 0.00274 and 0.747 μm for sulfate, 0.0132 and 8.88 μm for medium sea salt, 0.0221 and 19.8 μm for coarse sea salt.
[b]Dust models from *Kalashnikova et al.* [2005].
[c]Models from the MISR v17 Standard Algorithm.

Table 9. Patch Locations for the Four Representative MISR-AERONET Coincident BB Cases[a]

Case Group	1 (BB-Dominated)	2 (BB-Dust Mixed)	3 (BB-Dust Mixed)	4 (BB-Dust Mixed)
Site	Cuiaba-Miranda	Ilorin	Ouagadougou	Ilorin
MISR path	227	191	195	190
MISR block	103	84	81	84
Hazy day date	2001/08/31	2001/02/24	2000/12/18	2001/02/17
Overpass time (UTC)	14:16:13	10:31:41	10:56:28	10:25:44
Orbit	9061	6321	5331	6219
Clean day date	2001/07/30	2001/03/12	2001/01/19	2001/02/01 (2000/11/13)[b]
Overpass time (UTC)	14:17:10	10:30:52	10:55:39	10:25:57 (10:27:17)
Orbit	8595	6554	5797	5986 (4821)
AOD_A[a]	0.12 ± 0.00	0.61 ± 0.00	0.35 ± 0.01	0.41 ± 0.02 (0.22)[c]
P0	−15.72°N, −56.02°E	8.31°N, 4.33°E	12.18°N, −1.39°E	8.31°N, 4.33°E
P1	−15.59°N, −55.84°E	8.57°N, 4.67°E	12.36°N, −1.08°E	8.25°N, 4.60°E
P2	−15.56°N, −56.03°E	8.58°N, 4.35°E	12.37°N, −1.17°E	8.27°N, 4.75°E
P3	−15.40°N, −56.09°E	8.61°N, 4.06°E	12.11°N, −1.77°E	8.39°N, 4.71°E
P4	−15.60°N, −56.09°E	8.53°N, 4.01°E	11.99°N, −1.36°E	8.55°N, 4.30°E
P5	−15.85°N, −56.17°E	–	12.05°N, −1.38°E	8.58°N, 4.00°E
P6	−16.03°N, −56.01°E	–	12.14°N, −1.39°E	8.40°N, 3.67°E
P7	–	–	–	8.29°N, 4.10°E

[a]Coincident AERONET Version 2, level 1.5 AOD measurements. Reported values are the mean of all available measurements interpolated linearly between the nearest AERONET channel pairs, usually 440 or 500 nm and 675 nm; within ±1 hour of the MISR overflight.
[b]Surface RPV values for P0 in this case were not retrieved by the Standard Algorithm on 2001/02/01, so those retrieved on 2000/11/13, of which the orbital information is parenthesized, are used for P0 instead.
[c]No AERONET AOD measurement available. Reported value is MISR_v17 AOD.

Surface properties are especially difficult to retrieve under thick aerosol layers in hazy conditions. However, when the atmosphere is relatively clear, the TOA radiance comes primarily from the surface, especially at near-nadir view angles, yielding more accurate surface retrievals. For the Research Retrieval studies, to maximize surface characterization quality, we retrieve the surface RPV parameters for the targets of interest on the clearest, cloudless days having the same viewing geometry (i.e., the same Terra orbital "path"), and occurring as soon as possible before or after the hazy day orbit. (We call these "clean day orbits" hereafter.) With the assumption that the surface properties stay relatively constant over the period between the hazy and clean day orbits, the clean day RPV retrievals should provide more reliable surface characterization, especially for cases having hazy day AOD near or larger than unity.

[52] For the clean day surface retrievals, we constrain the atmospheric aerosols with coincident AERONET data (Table 8). The clean day surface RPV for each patch is retrieved as follows: first, the aerosol contributions to the TOA radiance is simulated by a forward RT model [e.g., *Kahn et al.*, 2005b], assuming AOD, size distribution, and SSA for all patches in the region equal the coincident AERONET inversions on that day; taking into account the aerosol contribution, we iterate the model over surface RPV parameter ranges, initialized by the RPV values retrieved by the MISR v17 Standard Retrievals, until the modeled equivalent reflectances fit the observed MISR equivalent reflectance well for each patch. The MISR orbits and the AERONET AOD on the clean days are also listed in Table 9.

[53] It should be noted that high optical depth conditions usually prevail for one to three months during the burning seasons, and are often followed immediately by cloudy and rainy seasons. This limits the availability of good clean days, so we had to balance temporal proximity to the hazy day against the desired low AOD conditions when selecting clean days. As a result, the clean day orbit 2001/03/12, chosen for Ilorin_20010224, and 2001/01/19, for Ouagadougou_20001218, have mid-visible AODs of 0.6 and 0.34, respectively. These AODs are only somewhat lower than the corresponding hazy days (0.884 and 0.530); yet these are the cleanest days available within a reasonable time range. In addition, surface RPV values for Ilorin on 2001/02/01 (which is the clean day for Ilorin_20010217) at patch P0 were not retrieved by the MISR Standard Algorithm; therefore RPV parameters retrieved on 2000/11/13 at P0 were used instead as the initial guess to start the iteration. This should not produce any significant difference in the derived clean day RPV, considering that the surface RPV values retrieved for nearby patches between 2001/02/01 and 2000/11/13 differed only by about 10%, and that the surface contribution dominates the TOA radiance under clear conditions.

5.2. MISR Research Retrievals of Selected Field Cases

[54] The results of Research Retrievals for the four chosen cases are present below. For each case, the patch having the lowest χ^2 values in the Research Retrieval is designated the "best patch", whereas the patches having χ^2 lower than 1.5 are denoted "accepted patches." Tables 10, 11, and 12 summarize the Research Retrieval results for AOD, size distribution, and SSA, respectively. In these tables, the Research Retrieval results for the best fit mixture of patch P0 (the exact of location of AERONET site) and of the best patch are shown, along with the range spanned by best fit mixtures of all accepted patches, the coincident AERONET measurements and the best fit MISR_v17 Standard Retrieval results for patch P0. Note that the P0 patch, though co-located with AERONET, may fail to meet the scene uniformity conditions required to achieve a good satellite aerosol retrieval result. Other, nearby patches can usually be found having much better surface characteristics for retrievals, and given differences in MISR and AERO-

Table 10. AOD at 558 nm and Angstrom Exponent From AERONET Measurements, MISR v17 Standard Retrieval and Research Retrieval Results, for the Four Coincident BB Cases[a]

Site Hazy Day Date	Cuiaba-Miranda 2001/08/31	Ilorin 2001/02/24	Ouagadougou 2000/12/18	Ilorin 2001/02/17
# of patches having $\chi^2 < 1.5$	5	3	3	5
Best χ^2 *in* research retrieval (patch #)	0.39 (P2)	0.88 (P1)	0.35 (P3)	0.54 (P1)
χ^2 in research retrieval at P0	6.56	1.24	1.38	6.83
Mid-visible AOD				
AERONET (AOD_A)	0.34 ± 0.01	0.88 ± 0.00	0.53 ± 0.01	1.74 ± 0.03
MISR_v17_3 × 3 (AOD_M)	0.30	0.63	0.43	0.78
Research-Best	0.35	1.00	0.50	1.55
Research-P0	0.45	0.75	0.40	2.00
(Research-Range)	(0.30–0.35)	(0.75–1.00)	(0.40–0.50)	(1.20–1.55)
Ångstrom Exponent				
AERONET ($\mathring{A}_A$)	1.82	0.52	0.41	0.41
MISR_v17_3 × 3 ($\mathring{A}_M$)	1.58	0.79	0.50	0.54
Research-best	1.86	0.72	0.79	0.78
Research-P0	1.69	1.47	1.33	0.71
(Research-range)	(1.74–2.03)	(0.72–1.47)	(0.79–1.40)	(0.44–0.78)

[a]AERONET = coincident AERONET Version 2, level 1.5 measurements. Reported values are the mean of all available measurements interpolated linearly between the nearest AERONET channel pairs, usually 440 or 500 nm and 675 nm; within ±1 hour of the MISR overflight for AOD, and ±2 hours for SSA and size distribution. MISR_v17 = best-fit mixture in the MISR v17 Standard Retrieval results for the 17.6 km region containing the AERONET site. Research = best-fit mixture from the Research Retrieval, using surface RPV derived for the corresponding clean day; results at the patch having the lowest χ^2 (Best), at patch P0, and the range spanned by best-mixtures in all patches having $\chi^2 < 1.5$ (−Range, parenthesized) are reported.

NET spatial-temporal sampling, are as likely to contain comparable aerosol properties.

5.2.1. Cuiaba-Miranda_20010831 (Case Group 1 — BB Dominated)

[55] For this biomass-dominated case, AERONET derives AOD_A of 0.34 and a high $\mathring{A}_A$ of 1.82. The MISR v17 retrieval slightly underestimates mid-visible AOD by 0.04 (around 12%) and Ångstrom Exponent by 0.24, compared to AERONET. Of the Research Algorithm results, the lowest χ^2 (0.39) occurs for patch P2; the retrieved AOD is 0.35, the same as the MISR v17 retrieval, and AOD retrieved at the four accepted patches ranges between 0.30 to 0.35, covering the values in both AERONET and MISR v17 (Table 10). (Note that the Research Retrieval was run with an AOD resolution of 0.05, so these results represent agreement.) The Research Retrieval Ångstrom Exponents range from 1.74 to 2.03 for the patches, higher than the MISR v17 results and bracketing the AERONET measurements. The comparisons of wavelength-dependent AOD retrievals are illustrated in

Table 11. Aerosol Fine Mode Fraction, Fine Mode Size, and Coarse Mode Size From AERONET Measurements, MISR v17 Standard Retrievals, and Research Retrieval Results, for the Four Coincident BB Cases

Site Hazy Day Date	Cuiaba-Miranda 2001/08/31	Ilorin 2001/02/24	Ouagadougou 2000/12/18	Ilorin 2001/02/17
Spherical AOD fraction at 558 nm				
AERONET	93%	44%	33%	35%
MISR_v17	100%	60%	40%	40%
Research-best	100%	80%	95%	60%
Research-P0	95%	95%	100%	85%
(Research-range)	(95–100%)	(80–100%)	(95–100%)	(50–60%)
Spherical particle size (μm) and fraction				
AERONET	0.10 ± 0.00 (93%)	0.06 ± 0.00 (44%)	0.06 ± 0.00 (33%)	0.06 ± 0.00 (35%)
MISR_v17	0.06, 80% 1.00, 20%	0.06 54% 1.00, 6%	0.06, 36% 1.00, 4%	0.06, 36% 1.00, 4%
Research-best	0.04, 40% 0.07, 15% 0.13, 15% 0.16, 30%	0.07, 5% 0.13, 10% 0.16, 65%	0.16, 95%	0.07, 30% 0.13, 25% 0.16, 5%
Research-P0	0.07, 60% 0.16, 35%	0.07, 40% 0.13, 45% 0.16, 10%	0.04, 5% 0.13, 80% 0.16, 15%	0.16, 85%
(Research-range)	(0.04, 15–40%) (0.07, 15–80%) (0.13, 0–60%) (0.16, 0–30%)	(0.07, 5–40%) (0.13, 10–45%) (0.16, 10–75%)	(0.04, 0–25%) (0.07, 0–10%) (0.13, 0–80%) (0.16, 15–95%)	(0.04, 0–10%) (0.07, 0–30%) (0.13, 25–50%) (0.16, 0–5%)
Nonspherical particle size (μm) and fraction				
AERONET	0.62 ± 0.02 (7%)	0.66 ± 0.04 (56%)	0.80 ± 0.01 (67%)	0.68 ± 0.05 (65%)
MISR_v17	– 0%	0.50, 40%	0.50, 60%	0.50, 60%
Research-best	– 0%	0.50, 20%	0.50, 5%	0.50, 40%
Research-P0	0.50, 5%	0.50, 5%	– 0%	1.00, 15%
(Research-range)	(0.50, 0–5%)	(0.50, 0–20%)	(0.50, 0–5%)	(0.50, 0–55%)

Table 12. Total and Fine Mode SSA and SSA Spectral Dependence From AERONET Measurements, MISR v17 Standard Retrieval, and Research Retrieval Results, for the Four Coincident BB Cases

Site Hazy day date	Cuiaba-Miranda 2001/08/31	Ilorin 2001/02/24	Ouagadougou 2000/12/18	Ilorin 2001/02/17
Total mid-visible SSA				
AERONET (SSA_A)	0.80 ± 0.01	0.92 ± 0.01	0.94 ± 0.00	0.93 ± 0.01
MISR_v17 (SSA_M)	0.92	1.00	0.99	0.99
Research-best	0.838	0.939	0.935	0.900
Research-P0	0.903	0.903	0.939	0.931
(Research-range)	(0.838–0.899)	(0.899–0.935)	(0.899–0.939)	(0.900–0.931)
SSA spectral dependence				
AERONET ($\alpha_{\omega_0}A$)	+0.16	−0.07	−0.07	−0.08
MISR_v17 ($\alpha_{\omega_0}M$)	+0.03	−0.01	−0.05	−0.05
Research-best	+0.07	0.00	+0.05	−0.08
Research-P0	+0.15	+0.06	+0.07	+0.02
(Research-range)	(+0.07 to +0.15)	(0.00 to +0.06)	(0.00 to +0.07)	(−0.11 to +0.02)

Figure 5a. The black solid line is the spectral AOD from AERONET, the black dashed line is the MISR v17 result, and the gray solid line and the gray dotted line are the Research Retrievals at the best patch and P0, respectively. There is close agreement among all the results for this case.

[56] AERONET inversions derive a dominant AOD fraction (93%) of fine mode particles with $r_{pg,N}$ around 0.10 μm, and 7% of coarse mode, around 0.62 μm in size (Table 11). Figure 6a compares the number size distribution of AERONET (green line), MISR v17 (blue line), and the Research Retrievals (red line for the best patch, yellow line for patch P0, and gray lines for the other accepted patches). The MISR v17 Algorithm retrieves a fine mode and coarse mode size of 0.06 and 1.0 μm, respectively, which is a reasonable match considering the sensitivity of the MISR size retrievals, and the limited number of particles the Standard Algorithm can consider in practice. In the Research Retrievals, the dominant fine mode size is 0.07 μm (15–80%) and 0.13 μm (0–60%), whereas the coarse mode size is 0.5 μm. The major difference in size retrievals between MISR v17 and the Research Retrievals is the fractionation of fine mode versus coarse mode; the fine mode fraction increases from 80% in MISR v17 to 95–100% in the Research Retrievals. This difference is within the 20% particle type retrieval uncertainty we found in the theoretical sensitivity study of

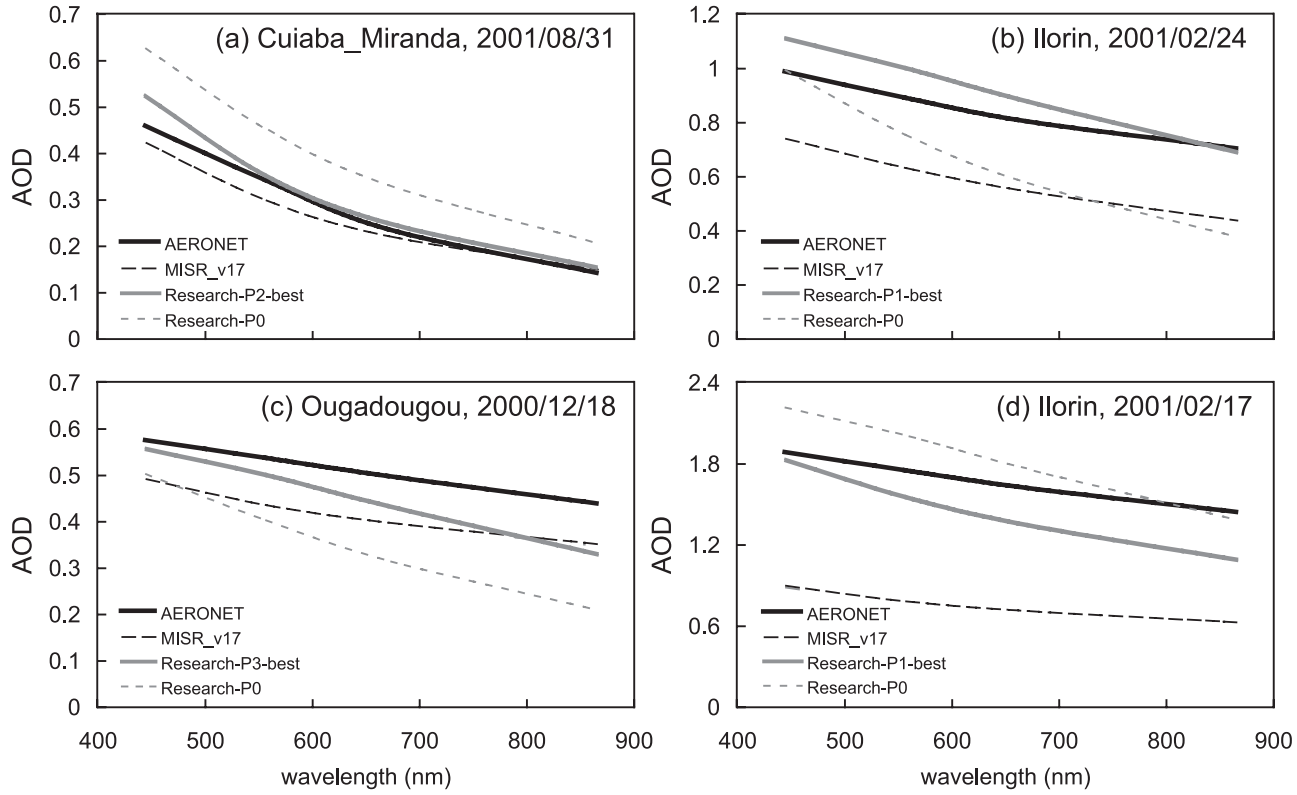

Figure 5. Spectral AOD for coincident AERONET measurements (black solid lines), best fit MISR v17 Standard Retrievals (black dashed lines), and best fit Research Retrievals for all patches (gray solid lines for patch with lowest χ^2, gray dotted lines for patch P0) for the four coincident BB cases.

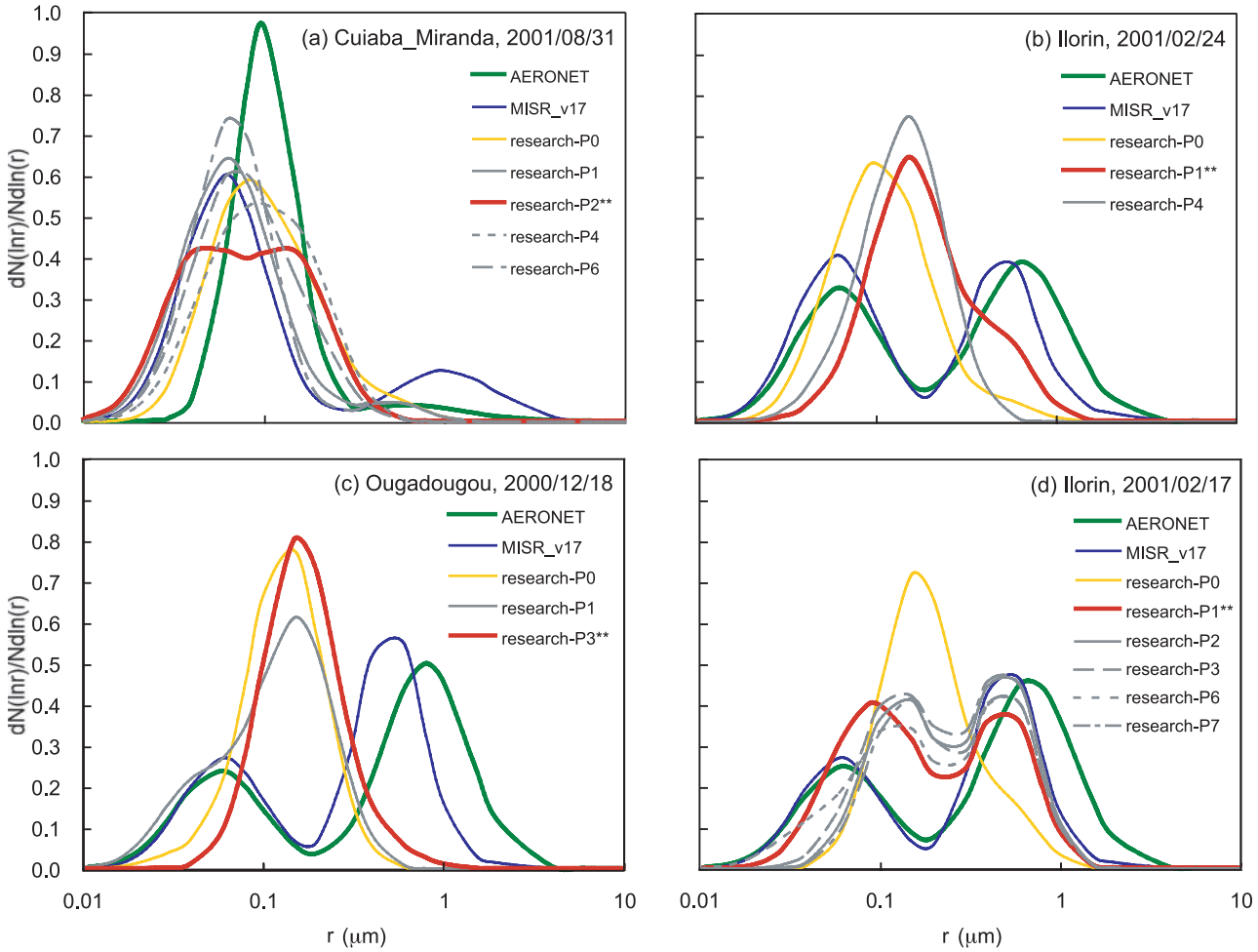

Figure 6. Normalized number size distributions for coincident AERONET measurements (green lines), best fit MISR v17 Standard Retrievals (blue lines), and best fit Research Retrievals (red lines for the best patch, yellow lines for P0, and gray lines for patches with $\chi^2 < 1.5$) for the four coincident BB cases. The best patch is also denoted by ** in the legend.

section 4, and it partially explains the higher Ångstrom Exponents in the Research Retrieval results.

[57] For SSA measurements, AERONET shows an absorbing SSS_A of 0.80, and a steep, positive $\alpha_{\omega_{0A}}$ of 0.16) (Table 12). Compared to AERONET, the MISR v17 Algorithm overestimates total mid-visible SSA by 0.12, and derives a flatter SSA spectral dependence ($\alpha_{\omega_{0M-A}} = -0.13$). These differences are in part a result of the limited selection of particles in the Standard Retrieval. The SSA obtained by the Research Retrievals is between 0.90 and 0.84, closer to AERONET than MISR v17. Recall that in the theoretical sensitivity study, MISR has low sensitivity to SSA for absorbing ($\omega_{0,558} \sim 0.84$) particles in small to medium (0.07–0.13 μm) sizes. The steepest slope, which is very close to that seen in AERONET, is retrieved at the best patch, where the lowest SSA of 0.84 is also retrieved. The retrieved SSA spectral slope ranges between 0.07 and 0.15 in the Research Retrievals, suggesting that scene variability, combined with sampling differences, may make a significant contribution to the MISR-AERONET differences in this case.

[58] Note that a high χ^2 value is derived at P0 by the Research Algorithm. TOA reflectances computed by the Research Algorithm from the given clean day surface and possible BB-dominated mixing groups all show too weak backward scattering and too strong forward scattering in all wavelengths, compared to the observations, which are responsible for the high χ^2 value. However, retrievals of particle size and SSA at P0 are still within the theoretical sensitivity range of those at the low-χ^2 patches, and therefore the high forward scattering in the computed TOA reflectances is more likely from the surface. Note that the spectral RPV parameters for P0 obtained for the clean day and hazy day orbits do not differ significantly. The P0 site was selected based on the AERONET location, not on meeting the surface uniformity criteria applied for the other retrieval patches, so the P0 surface properties may not be well characterized by the three-parameter RPV model. The uncertainty in aerosol retrievals due to surface characterization error can be identified and resolved by carrying out aerosol retrievals at a selection of nearby patches having similar surface properties, as done in this study. This should

be consideration when designing future Standard Retrieval algorithms.

5.2.2. Ilorin_20010224 (Case Group 2 — BB-Dust Mixed, 0.5 < AOD < 0.9)

[59] The second case has moderately high AOD with a BB-dust mixture, for which the AOD_A is 0.88 and $\mathring{A}_A$ is 0.52. The MISR v17 retrieval underestimates mid-visible AOD by 28%, and overestimates the Ångstrom Exponent by 0.27, compared to AERONET (Table 10). The best patch (P1), as determined by the Research Algorithm Retrieval χ^2 residuals, has AOD = 1.0, 14% higher than AERONET, and $\mathring{A}$ = 0.72, well within the sensitivity range of the AERONET value, based on the sensitivity study in section 4. Figure 5b shows that the Research Retrieval at the best patch has similar AOD spectral shape as MISR v17 but is closer in magnitude to AERONET; however, the spectral slope is somewhat steeper than AERONET. Results at P0 and P1 bracket the range of AOD and Ångstrom Exponent spanned by all three accepted patches, and suggest high spatial variability in the scene for this case.

[60] Although the MISR v17 Standard Algorithm retrieves similar fine mode size (0.06 μm), coarse mode size (0.5 μm dust), and fine mode fraction (54%) as that of AERONET (Figure 6b), retrieved mid-visible SSA in MISR v17 is much higher (SSA_M = 1.00, compared to SSA_A = 0.92), which at least partly explains the low bias in AOD_M. For an aerosol retrieval algorithm based on scattered light (e.g., MISR, MODIS), smaller AOD would be inferred to match the observed brightness if an overestimated SSA is adopted [*Kahn et al.*, 2005b]. The Research Retrieval, however, derives fine mode particle of larger size (0.13 to 0.16 μm) and 20–40% smaller fraction of 0.5 μm dust, compared to AERONET and MISR v17, but the mid-visible SSA (0.90 to 0.93) is closer to AERONET than MISR v17. In short, MISR v17 is close to AERONET in fine and coarse mode sizes and fraction, but is biased low in AOD and biased high in SSA; the Research Retrieval is close to AERONET in AOD, coarse mode size and SSA, but has larger fine mode size and smaller dust fraction. It should also be noted that the expected accuracy of the AERONET size distribution is 15–25% for radii over 0.5 μm. Both MISR and AERONET size distribution retrievals under dusty condition are yet to validated with independent field data [*Kalashnikova and Kahn*, 2006].

[61] Note that the components and mixtures retrieved by the MISR v17 Algorithm are all included in the comparison space of the Research Retrieval algorithm. In the Research Retrievals for all patches, the best fit mixtures have much better χ^2 values than that for the MISR v17 solution (χ^2 > 6). This is caused mainly by surface characterization differences, i.e., surface properties derived from hazy versus clean day data. In our three BB-dust mixed cases, the third RPV parameter (designated "b") derived from the clean day data generally exhibits a steeper spectral dependence and/or a more negative value, as shown in Figure 7. This indicates that a stronger backward scattering from the surface, especially in the shorter wavelengths, is retrieved on cleaner days. On hazy days having moderate to high AOD, however, some forward scattering from the aerosols may be inaccurately attributed to the surface. Therefore when the clean day surface is used, to match the observed hazy day TOA reflectances, stronger forward scattering in shorter wavelengths from the atmosphere is required. This explains the lower dust fraction derived in the Research Retrieval, since the spectral asymmetry factors (positive, i.e., forward scattering) for the BB spherical models are higher in short wavelengths, whereas the opposite is true for the dust models. The retrieval matches the observed brightness by combining higher total scattering from more fine mode particles with a larger fine mode particle size.

[62] Also note that, based on the theoretical sensitivity results, MISR has only moderate sensitivity to the fine mode components selected by the Research Retrieval; the range of fine mode size (0.13 to 0.16 μm) and mid-visible SSA (0.90 to 0.93) retrieved by the Research Algorithm are consistent with the 20% sensitivity range in the theoretical sensitivity for an atmosphere consisting of a medium, less absorbing component (i.e., Particle #11 in Table 5: $r_{pg,N}$ = 0.13 μm and $\omega_{0.558}$ = 0.90) with AOD = 0.5. On the other hand, for column AOD > 0.5, MISR is expected to have high sensitivity (especially in size) to the fine mode particle retrieved by AERONET ($r_{pg,N} \sim 0.06$ μm, $SSA_A \sim 0.92$), and even though similar components (e.g., Particles #10 and #14) are included in the comparison space, only <15% fractional AOD is retrieved by the Research Algorithm (except at P0). With the agreement in AOD and SSA between AERONET and the Research Retrievals, the difference in fine mode size and dust fraction is well within observational uncertainty, considering the differences in AERONET and MISR Research Retrieval Algorithm representative dust models, the sampling difference between the instruments, and the spatial variability in this case.

5.2.3. Ouagadougou_20001218 (Case Group 3 — BB-Dust Mixed, AOD < 0.5)

[63] For this low AOD, BB-dust mixture case, there is a slight AOD underestimation by MISR v17 (AOD_M = 0.43) relative to AERONET (AOD_A = 0.53), and a slight overestimation of Ångstrom Exponent ($\mathring{A}_M$ = 0.50, $\mathring{A}_A$ = 0.41). In the Research Retrievals, moderate spatial variability is observed for this case. τ_{558} at the best patch (P3) is 0.5, in better agreement with AERONET than MISR v17, whereas the range spanned by all accepted patches is from 0.4 to 0.5. Ångstrom Exponent at all four accepted patches in the Research Retrieval is higher than AERONET and MISR v17 (from 0.79 to 1.49). The AOD spectrum in Figure 5c shows that, although AODs from the Research Retrieval at the best patch are closer to AERONET measurements in the blue and green channels, underestimation occurs at longer wavelengths, but the results are overall within the range of expected sensitivity.

[64] Size and SSA retrievals are similar to those seen in the second case. The MISR v17 Algorithm obtains good agreement in size distribution and fine mode fraction (Table 11 and Figure 6c), but retrieves a nearly non-absorbing mid-visible SSA (0.99, Table 12) owing to the lack of absorbing fine mode components in the solution space. The Research Retrievals derive larger fine mode particles ($r_{pg,N}$ = 0.13–0.16 μm) and higher fine mode fraction (95–100%) for all accepted patches because the clean day surface was used (Figure 7b). There is improved agreement in mid-visible SSA (0.899–0.935) to AERONET (SSA_A = 0.94), although the SSA spectral slope in the Research Retrievals (+0.05 to +0.07) does not agree with AERONET (−0.07) as well as MISR v17 (−0.05) does.

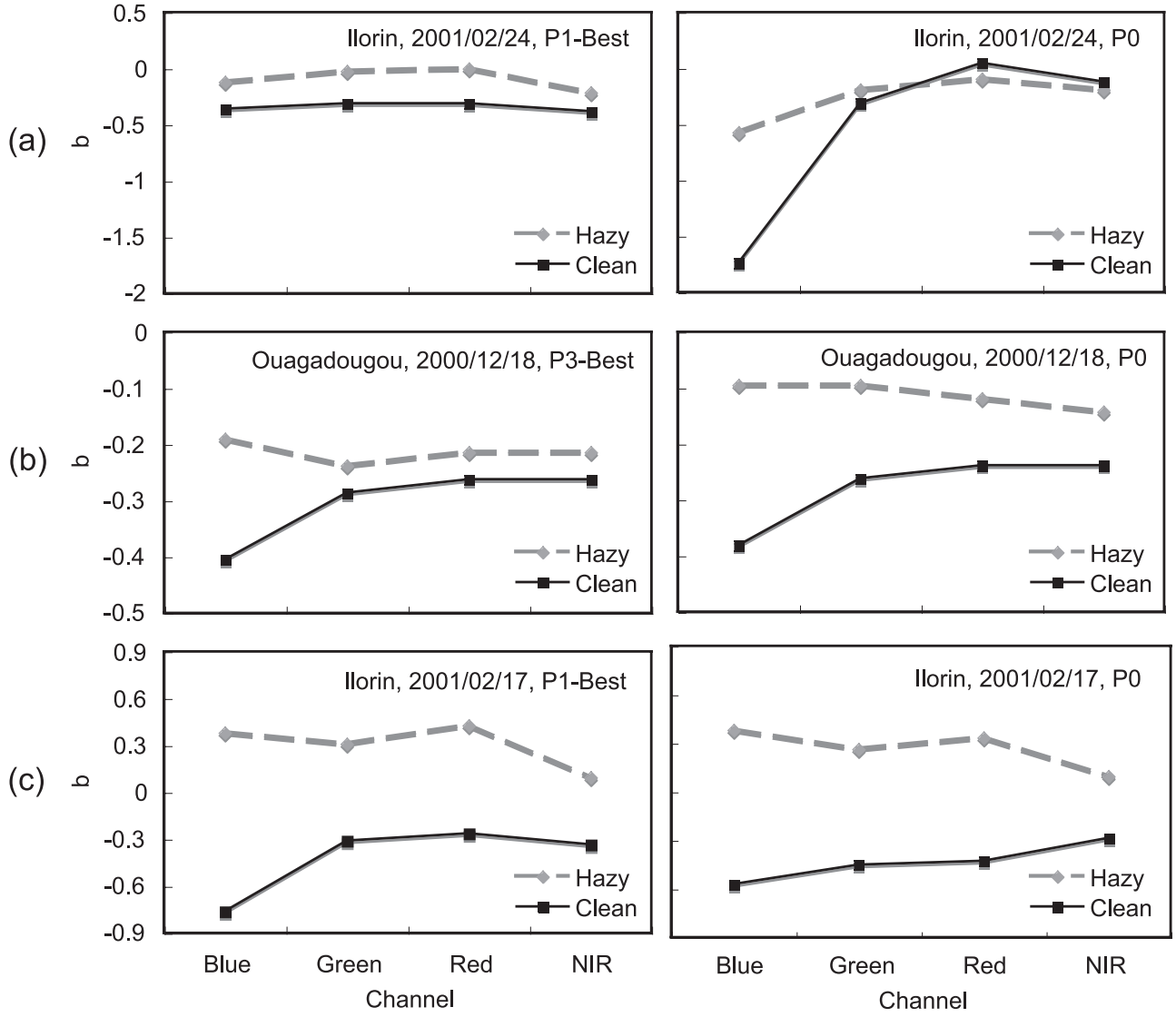

Figure 7. The third surface RPV parameter retrieved by the MISR v17 Standard Algorithm at all four MISR channels for hazy day (gray dashed lines) and the clean day orbit (black solid lines) for (a) Ilorin_2001/02/24, (b) Ouagadougou_2000/12/18, and (c) Ilorin_2001/02/17. For each case, plots are shown for the best patch (left) and for P0 (right).

Again, considering the complexity of aerosol retrieval over land, the size and SSA retrieved by MISR and AERONET can exhibit similar levels of uncertainty.

5.2.4. Ilorin_20010217
(Case Group 4 — BB-Dust Mixed, AOD > 0.9)

[65] For this extremely high AOD case (AOD_A = 1.74) containing BB-dust mixtures, the most significant discrepancy in the MISR v17 retrievals is the underestimation of AOD by 0.96 (55%), which we expect is associated with difficulties in separating surface and atmospheric contributions to the satellite signals. The first surface RPV parameters (not shown) for clean day orbit, which roughly characterize brightness, are 55–70% less in all eight patches than those retrieved by the Standard Algorithm on the hazy day. The third RPV parameters (Figure 7c) are also more negative for the clean day orbit, indicating more forward scattering should be attributed to the atmosphere. The use of clean day surface RPV in the Research Retrieval effectively eliminates the large low bias in AOD_M. The mid-visible AOD retrieved by the Research Algorithm is much closer to the AERONET value for all patches: 2.0 at patch P0 with a very high χ^2 of 6.83, and 1.55 at the best patch (P1). The range spanned by all the accepted patches is between 1.2 to 1.55. Figure 5d shows that the Research Algorithm obtains better agreement in the AOD magnitude, but steeper spectral slopes (higher Ångstrom Exponent), whereas the MISR v17 retrievals derive much lower AOD in all wavelengths, but Ångstrom Exponents closer to the AERONET measurements.

[66] Table 11 and Figure 6d show that MISR v17 matches the AERONET size distribution well, capturing the two modes of 0.06 and 0.68 μm with a fine mode fraction of around 35%. The accepted patches in the Research Retrievals (pink line and gray lines in Figure 6d also show reasonable agreements with AERONET, having a larger fine mode size (0.07–0.13 μm), a coarse mode size of

0.5 μm, and slightly higher fine mode fraction (50–60%). The MISR v17 retrievals derive a nearly non-absorbing mid-visible SSA (0.99, Table 12), whereas the Research Retrievals agree closely with AERONET (SSA_A = 0.93), having a range between 0.90 and 0.92. SSA spectral slopes retrieved by the MISR v17 Standard Algorithm (−0.05) and by the Research Algorithm (−0.08 to −0.11) both match the value measured by AERONET (−0.08) fairly well. The results of lower dust fraction, larger fine mode, and better SSA agreement to AERONET are similar to the results in the previous two cases, and may represent similar uncertainty for size and SSA retrievals in an atmosphere containing mixtures of BB and dust particles.

6. Summary and Conclusions

[67] Biomass burning aerosols, because they are optically absorbing and highly variable spatially and temporally, are among the most uncertain climate forcing agents. The global multiangle, multispectral measurements made by the MISR instrument provide valuable information that can help improve our understanding of this important tropospheric constituent. To obtain as much information from the algorithm, and to ensure correct interpretation of the results, we systematically explored instrument sensitivity to particle properties, and assessed the performance of those component properties assumed in the instrument's Standard Algorithm.

[68] Classifying coincident MISR and AERONET cases at major BB sites revealed distinct patterns of AOD and SSA discrepancies. Analyses of cases in each of four classes led to suggestions for specific refinements of the current MISR Standard Aerosol Retrieval Algorithm: the need to add to the algorithm particle climatology (1) absorbing particles having steeper SSA spectral dependence and (2) mixtures of dust and absorbing spherical particles. The comparison also shows the importance of refining the Standard algorithm surface representation for aerosol retrievals in some situations, when the mid-visible AOD exceeds about 0.5.

[69] As reviewed in section 3, measurements from past BB field campaigns have established relationships between BB aerosol microscopical and optical properties, as well as vegetation type, plume age, and fire phase. On the basis of our theoretical sensitivity study covering the observed range of BB particle size and mid-visible SSA, with about 20 percent uncertainty in fractional, mid-visible column AOD, MISR is able to differentiate particles in two to three categories each of size (very small to small, medium, large) and SSA (very absorbing, absorbing, weakly to less absorbing) over dark surfaces. The detailed result depends on the actual size distribution and SSA of the atmospheric component. For a total column AOD of 0.2 or less, MISR has poor sensitivity to size and SSA when the assumed atmospheric particles are absorbing or of medium sizes, but increases considerably when the column AOD is raised to 0.5. The retrieved total column AOD is constrained to at least ±0.05 for these situations.

[70] Research Retrievals were carried out for representative cases, with the proposed BB components and mixtures and importantly, with prescribed surface properties derived on days having relatively low aerosol loading. AOD from the MISR Research Retrieval for the patches having the best fitting results were consistently in better agreement with AERONET than the MISR v17 Standard Retrievals. For cases with AOD < 1.0, retrieved AODs were within 14%, whereas for the extreme case with AOD ~ 1.7, the Research Algorithm constrained the AOD to within 0.19 (11%), even when the MISR and AERONET particle properties did not agree well.

[71] For the BB-dominated example, in addition to the improved AOD results, size, SSA, and α_{ω_0} retrievals were in agreement with AERONET, and the size and SSA retrieval sensitivity was similar to that in the theoretical study. In the three mixed BB-dust cases, the atmosphere consisted of a bi-modal distribution containing an absorbing, spherical fine mode component and a comparable amount of a coarse mode component. Also, high spatial variability of aerosol amount and properties was evident from Research Retrieval results over multiple, closely spaced patches. The Research Retrievals derived a larger fine mode size and lower coarse mode fraction than AERONET, but showed closer agreement in SSA. The difference in fine mode size and fraction can be attributed to the combination of uncertainties in surface characterization, representative non-spherical particle modeling for both MISR and AERONET, sampling differences, and spatial variability.

[72] The MISR results can be compared with the validation studies performed for Moderate Resolution Imaging Spectroradiometer (MODIS) BB aerosol retrievals over land. MODIS AOD retrieval results are sensitive to the prescribed particle SSA, which, unlike MISR, is not constrained by observations in the retrieval process, but is assigned a priori to each geographic region as a function of season [*Remer et al.*, 2005; *Levy et al.*, 2007b]. *Ichoku et al.* [2003] found that lowering the mid-visible SSA from 0.90 to 0.86 essentially eliminates the prevailing low bias of MODIS AOD (compared to AERONET) during SAFARI 2000. Our case study showed that the spectral dependence of SSA is also an important parameter for retrieving BB particles. When particle models with steeper SSA spectral slopes, as observed under ambient conditions, are included in the Research Retrieval Algorithm particle climatology, the high bias in retrieved SSA and low bias in AOD in the MISR Standard Retrievals were simultaneously eliminated for the BB-dominated cases.

[73] *Mi et al.* [2007] evaluated the MODIS AOD retrievals over land at two AERONET sites in China. They found that the recently released Collection 5 MODIS aerosol land algorithm (C005), which uses a more sophisticated assumption for surface reflectance (as a function of vegetation type and scattering angle) and spheroidal models for representative dust particles [*Levy et al.*, 2007a], retrieves AODs in better agreement to AERONET than the previous C004 algorithm, which uses a fixed surface reflectance ratio and spherical coarse models. The results by *Mi et al.* [2007] cannot be compared directly to this study, because of the large differences between the MODIS and MISR instruments and retrieval algorithms. However, our results for the mixed BB-dust case with extremely high AOD, and the comparisons among patches with different surface conditions for each case, also demonstrate the importance of detailed and accurate surface characterization for successfully retrieving aerosol amount and properties over land. New strategies for

constraining surface properties should be considered when aerosol retrieval algorithms are developed for the future.

[74] **Acknowledgments.** We thank the AERONET network site managers for granting the use of AERONET data, and Alexander Smirnov for many helpful suggestions on AERONET data quality. The authors gratefully acknowledge the NOAA Air Resources Laboratory (ARL) for providing the HYSPLIT transport and dispersion model used in this publication. The authors also thank Barbara Gaitley at the Jet Propulsion Laboratory (JPL), California Institute of Technology (Caltech), for the help in processing the MISR-AERONET coincident data, and y and Michael Bull at JPL, Caltech for advice regarding the MISR standard aerosol retrieval algorithm implementation. The work of R. Kahn, K. Yau, and D. Nelson is supported in part by NASA's Climate and Radiation Research and Analysis Program, under H. Maring, NASA's Atmospheric Composition Program under P. DeCola, and the EOS-MISR instrument project; it is performed at the JPL, Caltech, under contract with NASA, and at the NASA Goddard Space Flight Center.

References

Abel, S., J. M. Haywood, E. J. Highwood, J. Li, and P. R. Buseck (2003), Evolution of biomass burning aerosol properties from an agricultural fire in south Africa, *Geophys. Res. Lett.*, *30*(15), 1783, doi:10.1029/2003GL017342.

Ackerman, T. P., A. J. Braverman, D. J. Diner, T. L. Anderson, R. A. Kahn, J. V. Martonchik, J. E. Penner, P. J. Rasch, B. A. Wielicki, and B. Yu (2004), Integrating and interpreting aerosol observations and models within the PARAGON framework, *Bull. Am. Meteorol. Soc.*, *85*, 1523–1533.

Anderson, B. E., W. B. Grant, G. L. Gregory, E. V. Browell, J. E. Collins Jr., G. W. Sachse, D. R. Bagwell, C. H. Hudgins, D. R. Blake, and N. J. Blake (1996), Aerosols from biomass burning over the tropical South Atlantic region: Distributions and impacts, *J. Geophys. Res.*, *101*(D19), 24,117–24,137.

Andreae, M. O., and P. Merlet (2001), Emission of trace gases and aerosols from biomass burning, *Global Biogeochem. Cycles*, *15*(4), 955–966.

Bergstrom, R. W., P. Pilewskie, B. Schmid, and P. B. Russell (2003), Estimates of the spectral aerosol single scattering albedo and aerosol radiative effects during SAFARI 2000, *J. Geophys. Res.*, *108*(D13), 8474, doi:10.1029/2002JD002435.

Bond, T. C., and R. W. Bergstrom (2006), Light absorption by carbonaceous particles: An investigative review, *Aerosol Sci. Technol.*, *40*, 27–67.

Bond, T. C., D. G. Streets, K. F. Yarber, S. M. Nelson, J.-H. Woo, and Z. Klimont (2004), A technology-based global inventory of black and organic carbon emissions from combustion, *J. Geophys. Res.*, *109*(D14), D14203, doi:10.1029/2003JD003697.

Collins, W. D., P. J. Rasch, B. E. Eaton, B. V. Khattatov, J.-F. Lamarque, and C. S. Zender (2001), Simulating aerosols using a chemical transport model with assimilation of satellite aerosol retrievals: Methodology for INDOEX, *J. Geophys. Res.*, *106*(D7), 7313–7336.

Diner, D. J., et al. (1998), Multi-angle imaging spectroradiometer (MISR) instrument description and experiment overview, *IEEE Trans. Geosci. Remote Sens.*, *36*, 1072–1087.

Diner, D. J., et al. (2001), MISR level 2 aerosol retrieval algorithm theoretical basis, Rep. JPL D-11400, Rev. E, Jet Propul. Lab., Pasadena, Calif.

Draxler, R. R., and G. D. Rolph (2003), HYSPLIT (HYbrid Single-Particle Lagrangian Integrated Trajectory) model access via NOAA ARL READY Website (http://www.arl.noaa.gov/ready/hysplit4.html), NOAA Air Resources Laboratory, Silver Spring, MD.

Dubovik, O., B. N. Holben, Y. J. Kaufman, M. Yamasoe, A. Smirnov, D. Tanré, and I. Slutsker (1998), Single-scattering albedo of smoke retrieved from the sky radiance and solar transmittance measured from ground, *J. Geophys. Res.*, *103*(D24), 31,903–31,923.

Dubovik, O., A. Smirnov, B. N. Holben, M. D. King, Y. J. Kaufman, T. F. Eck, and I. Slutsker (2000), Accuracy assessments of aerosol optical properties retrieved from Aerosol Robotic Network (AERONET) sun and sky radiance measurements, *J. Geophys. Res.*, *105*, 9791–9806.

Dubovik, O., B. N. Holben, T. F. Eck, A. Smirnov, Y. J. Kaufman, M. D. King, D. Tanré, and I. Slutsker (2002), Variability of absorption and optical properties of key aerosol types observed in worldwide locations, *J. Atmos. Sci.*, *59*, 590–608.

Duncan, B. N., R. V. Martin, A. C. Staudt, R. Yevich, and J. A. Logan (2003), Interannual and seasonal variability of biomass burning emissions constrained by satellite observations, *J. Geophys. Res.*, *108*(D2), 4100, doi:10.1029/2002JD002378.

Eck, T. F., B. N. Holben, I. Slutsker, and A. Setzer (1998), Measurements of irradiance attenuation and estimation of aerosol single scattering albedo for biomass burning aerosols in Amazonia, *J. Geophys. Res.*, *103*(D24), 31,865–31,878.

Eck, T. F., B. N. Holben, J. S. Reid, N. T. O'Neill, J. S. Schafer, O. Dubovik, A. Smirnov, M. A. Yamasoe, and P. Artaxo (2003a), High aerosol optical depth biomass burning events: a comparison of optical properties for different source regions, *Geophys. Res. Lett.*, *30*(20), 2035, doi:10.1029/2003GL017861.

Eck, T. F., et al. (2003b), Variability of biomass burning aerosol optical characteristics in southern Africa during the SAFARI 2000 dry season campaign and a comparison of single scattering albedo estimates from radiometric measurements, *J. Geophys. Res.*, *108*(D13), 8477, doi:10.1029/2002JD002321.

Einfeld, W., D. E. Ward, and C. C. Hardy (1991), Effects of fire behavior on prescribed fire smoke characteristics: A case study, in *Global Biomass Burning: Atmospheric, Climatic, and Biospheric Implications*, edited by J. S. Levine, pp. 412–419, MIT Press, Cambridge, Mass.

Formenti, P., W. Elbert, W. Maenhaut, J. Haywood, S. Osborne, and M. O. Andreae (2003), Inorganic carbonaceous aerosols during the Southern African Regional Science Initiative (SAFARI 2000) experiment: Chemical characteristics, physical properties, and emission data for smoke from African biomass burning, *J. Geophys. Res.*, *108*(D13), 8488, doi:10.1029/2002JD002408.

Forster, P., et al. (2007), Changes in atmospheric constituents and in radiative forcing, in *Climate Change 2007: The Physical Science Basis, Contribution of Working Group I to the Fourth Assessment Report of the Intergovernmental Panel on Climate Change*, edited by S. Solomon et al., pp. 129–234, Cambridge Univ. Press, Cambridge, U.K.

Guyon, P., B. Graham, J. Beck, O. Boucher, E. Gerasopoulos, O. L. Mayol-Bracero, G. C. Roberts, P. Artaxo, and M. O. Andreae (2003), Physical properties and concentration of aerosol particles over the Amazon tropical forest during background and biomass burning conditions, *Atmos. Chem. Phys.*, *3*, 951–967.

Grant, I. P., and G. E. Hunt (1968), Solution of radiative transfer problems using invariant Sn method, *Mon. Not. R. Astron. Soc.*, *141*, 1–27.

Haywood, J. M., P. N. Francis, O. Dubovik, M. Glew, and B. N. Holben (2003a), Comparison of aerosol size distributions, radiative properties, and optical depths determined by aircraft observations and Sun photometers during SAFARI 2000, *J. Geophys. Res.*, *108*(D13), 8471, doi:10.1029/2002JD002250.

Haywood, J. M., S. R. Osborne, P. N. Francis, A. Keil, P. Formenti, M. O. Andreae, and P. H. Kaye (2003b), The mean physical and optical properties of regional haze dominated by biomass burning aerosol measured from the C-130 aircraft during SAFARI 2000, *J. Geophys. Res.*, *108*(D13), 8473, doi:10.1029/2002JD002226.

Hobbs, P. V., J. S. Reid, J. A. Herring, J. D. Nance, R. E. Weiss, J. L. Ross, D. A. Hegg, R. D. Ottmar, and C. Liousse (1996), Particle and trace-gas measurements in the smoke from prescribed burns of forest products in the Pacific Northwest, in *Biomass Burning and Global Change*, edited by J. S. Levine, pp. 697–715, MIT Press, Cambridge, Mass.

Hobbs, P. V., J. S. Reid, R. A. Kotchenruther, R. J. Ferek, and R. Weiss (1997), Direct radiative forcing by smoke from biomass burning, *Science*, *275*, 1776–1778.

Holben, B. N., Y. J. Kaufman, A. W. Setzer, D. D. Tanré, and D. E. Ward (1991), Optical properties of aerosol emissions from biomass burning in the Tropics, BASE-A, in *Global Biomass Burning: Atmospheric, Climatic and Biospheric Implications*, edited by J. S. Levine, pp. 403–411, MIT Press, Cambridge, Mass.

Holben, B. N., et al. (1998), AERONET: A federated instrument network and data archive for aerosol characterization, *Remote Sens. Environ.*, *66*, 1–16.

Ichoku, C., L. A. Remer, Y. J. Kaufman, R. Levy, D. A. Chu, D. Tanré, and B. N. Holben (2003), MODIS observation of aerosols and estimation of aerosol radiative forcing over southern Africa during SAFARI 2000, *J. Geophys. Res.*, *108*(D13), 8499, doi:10.1029/2002JD002366.

Iziomon, M. G., and U. Lohman (2003), Optical and meteorological properties of smoke-dominated haze at the ARM Southern Great Plains Central Facility, *Geophys. Res. Lett.*, *30*(3), 1123, doi:10.1029/2002GL016606.

Kahn, R. A., R. West, D. McDonald, B. Rheingans, and M. I. Mishchenko (1997), Sensitivity of multiangle remote sensing observations to aerosol sphericity, *J. Geophys. Res.*, *102*(D14), 16861–16870.

Kahn, R. A., P. Banerjee, D. McDonald, and D. J. Diner (1998), Sensitivity of multiangle imaging to aerosol optical depth and to pure-particle size distribution and composition over ocean, *103*(D24), 32,195–32,213.

Kahn, R. A., P. Banerjee, and D. McDonald (2001), Sensitivity of multiangle imaging to natural mixtures of aerosols over ocean, *J. Geophys. Res.*, *106*(D16), 18,219–18,238.

Kahn, R. A., B. Gaitley, J. V. Martonchik, D. J. Diner, K. A. Crean, and B. N. Holben (2005a), MISR global aerosol optical depth validation based on two years of coincident AERONET observations, *J. Geophys. Res.*, *110*, D10S04, doi:10.1029/2004JD004706.

Kahn, R. A., et al. (2005b), MISR low-light-level calibration, and implications for aerosol retrieval over dark water, *Atmos. J. Sci.*, *62*, 1032–1062.

Kalashnikova, O., and R. A. Kahn (2006), Ability of multiangle remote sensing observations to identify and distinguish mineral dust types: 2. Sensitivity over dark water, *J. Geophys. Res.*, *111*, D11207, doi:10.1029/2005JD006756.

Kalashnikova, O., R. A. Kahn, I. N. Sokolik, and W.-H. Li (2005), Ability of multiangle remote sensing observations to identify and distinguish mineral dust types: Optical models and retrievals of optically thick plumes, *J. Geophys. Res.*, *110*(D18), D18S14, doi:10.1029/2004JD004550.

Kreidenweis, S. M., L. A. Remer, R. Bruintjes, and O. Dubovik (2001), Smoke aerosol from biomass burning in Mexico: Hygroscopic smoke optical model, *J. Geophys. Res.*, *106*(D5), 4831–4844.

Le Canut, P., M. O. Andreae, G. W. Harris, F. G. Wienhold, and T. Zenker (1996a), Aerosol optical properties over southern Africa during SAFARI-92, in *Biomass Burning and Global Change*, edited by J. S. Levine, pp. 441–459, MIT Press, Cambridge, Mass.

Le Canut, P., M. O. Andreae, G. W. Harris, F. G. Wienhold, and T. Zenker (1996b), Airborne studies of emissions from savanna fires in southern Africa 1. Aerosol emission measured with a laser optical particle counter, *J. Geophys. Res.*, *101*(D19), 23,615–23,630.

Levy, R. C., L. A. Remer, S. Mattoo, E. Vermote, and Y. J. Kaufman (2007a), Second-generation operational algorithm: Retrieval of aerosol properties over land from inversion of Moderate Resolution Imaging Spectroradiometer spectral reflectance, *J. Geophys. Res.*, *112*, D13211, doi:10.1029/2006JD007811.

Levy, R. C., L. A. Remer, and O. Dubovik (2007b), Global aerosol optical models and application to MODIS aerosol retrieval over land, *J. Geophys. Res.*, *112*, D13210, doi:10.1029/2006JD007815.

Magi, B. I., P. V. Hobbs, B. Schmid, and J. Redemann (2003), Vertical profile of light scattering, light absorption, and single-scattering albedo during the dry, biomass burning season in southern Africa and comparisons of in situ and remote sensing measurements of aerosol optical depth, *J. Geophys. Res.*, *108*(D13), 8504, doi:10.1029/2002JD002361.

Martins, J. V., P. Artaxo, P. V. Hobbs, C. Liousse, H. Cashier, Y. J. Kaufman, and A. Plana-Fattori (1996), Particle size distributions, elemental compositions, carbon measurements, and optical properties of smoke from biomass burning in the Pacific Northwest of the United States, in *Biomass Burning and Global Change*, edited by J. S. Levine, pp. 716–732, MIT Press, Cambridge, Mass.

Martins, J. V., P. Artaxo, C. Liousse, J. S. Reid, P. V. Hobbs, and Y. J. Kaufman (1998), Effects of black carbon content, particle size, and mixing on light absorption by aerosols from biomass burning in Brazil, *J. Geophys. Res.*, *103*(D24), 32,041–32,050.

Martonchik, J. V., D. J. Diner, R. A. Kahn, T. P. Ackerman, M. M. Verstraete, B. Pinty, and H. R. Gordon (1998), Techniques for the retrieval of aerosol properties over land and ocean using multiangle imaging, *IEEE Trans. Geosci. Remote Sens.*, *36*, 1212–1227.

Martonchik, J. V., D. J. Diner, K. A. Crean, and M. A. Bull (2002), Regional aerosol retrieval results from MISR, *IEEE Trans. Geosci. Remote Sens.*, *40*, 1520–1531.

Mi, W., Z. Li, X. Xia, B. N. Holben, R. C. Levy, F. Zhao, H. Chen, and M. Cribb (2007), Evaluation of the Moderate Resolution Imaging Spectroradiometer aerosol products at two Aerosol Robotic Network stations in China, *J. Geophys. Res.*, *112*, D22S08, doi:10.1029/2007JD008474.

Miller, J. R., and N. T. O'Neill (1997), Multi-altitude airborne observations of isolation effects of forest fire smoke aerosols at BOREAS: Estimates of aerosol optical parameters, *J. Geophys. Res.*, *102*(D24), 29,729–29,736.

Petters, M. D., A. J. Prenni, S. M. Kreidenweis, P. J. DeMott, A. Matsunaga, Y. B. Lim, and P. J. Ziemann (2006), Chemical aging and the hydrophobic-to-hydrophilic conversion of carbonaceous aerosol, *Geophys. Res. Lett.*, *33*(24), L24806, doi:10.1029/2006GL027249.

Pilewskie, P., J. Pommier, R. W. Bergstrom, W. Gore, S. Howard, M. Rabbette, B. Schmid, P. V. Hobbs, and S. C. Tsay (2003), Solar spectral radiative forcing during the Southern African regional science Initiative, *J. Geophys. Res.*, *108*(D13), 8486, doi:10.1029/2002JD002411.

Pósfai, M., R. Simonics, J. Li, P. V. Hobbs, and P. R. Buseck (2003), Individual aerosol particles from biomass burning in southern Africa: 1. Compositions and size distributions of carbonaceous particles, *J. Geophys. Res.*, *108*(D13), 8483, doi:10.1029/2002JD002291.

Radke, L. F., D. A. Hegg, J. H. Lyons, C. A. Brock, P. V. Hobbs, R. Weiss, and R. Rassmussen (1988), Airborne measurements on smokes from biomass burning, in *Aerosols and Climate*, edited by P. V. Hobbs and M. P. McCormick, pp. 411–422, Deepak Publishing, Hampton, VA.

Radke, L. F., D. A. Hegg, P. V. Hobbs, J. D. Nance, J. H. Lyons, K. K. Laursen, R. E. Weiss, P. J. Riggan, and D. E. Ward (1991), Particulate and trace gas emissions from large biomass fires in North America, in *Global Biomass Burning: Atmospheric, Climatic and Biospheric Implications*, edited by J. S. Levine, pp. 209–224, MIT Press, Cambridge, Mass.

Rahman, H., B. Pinty, and M. Verstraete (1993), Coupled surface atmosphere reflectance (CSAR) model, 2, Semiempirical surface model usable with NOAA advanced very high resolution radiometer data, *J. Geophys. Res.*, *98*(D11), 20,791–20,801.

Reid, J. S., and P. V. Hobbs (1998), Physical and optical properties of young smoke from individual biomass fires in Brazil, *J. Geophys. Res.*, *103*(D24), 32,013–32,030.

Reid, J. S., P. V. Hobbs, C. Liousse, J. V. Martins, R. E. Weiss, and T. F. Eck (1998a), Comparisons of techniques for measuring shortwave absorption and black carbon content of aerosols from biomass burning in Brazil, *J. Geophys. Res.*, *103*(D24), 32,031–32,040.

Reid, J. S., P. V. Hobbs, R. J. Ferek, D. K. Blake, J. V. Martins, M. R. Dunlap, and C. Liousse (1998b), Physical, chemical, and optical properties of regional hazes dominated by smoke in Brazil, *J. Geophys. Res.*, *103*(D24), 32,059–32,080.

Reid, J. S., T. F. Eck, S. A. Christopher, P. V. Hobbs, and B. N. Holben (1999), Use of the Ångstrom exponent to estimate the variability of optical and physical properties of aging smoke particles in Brazil, *J. Geophys. Res.*, *104*(D22), 27,473–27,489.

Reid, J. S., R. Koppmann, T. F. Eck, and D. P. Eleuterio (2004a), A review of biomass burning emissions, Part II: Intensive physical properties of biomass burning particles, *Atmos. Chem. Phys. Discuss.*, *4*, 5135–5200.

Reid, J. S., T. F. Eck, S. A. Christopher, R. Koppmann, O. Dubovik, D. P. Eleuterio, B. N. Holben, E. A. Reid, and J. Zhang (2004b), A review of biomass burning emissions, Part III: Intensive optical properties of biomass burning particles, *Atmos. Chem. Phys. Discuss.*, *4*, 5201–5260.

Remer, L. A., Y. J. Kaufman, B. N. Holben, A. M. Thompson, and D. McNamara (1998), Biomass burning aerosol size distribution and modeled optical properties, *J. Geophys. Res.*, *103*(D24), 31,879–31,891.

Remer, L. A., et al. (2005), The MODIS aerosol algorithm, products, and validation, *J. Atmos. Sci.*, *62*(4), 947–973.

Sinyuk, A., et al. (2007), Simultaneous retrieval of aerosol and surface properties from a combination of AERONET and satellite data, *Remote Sens. Environ.*, *107*, 90–108, doi:10.1016/j.rse.2006.07.022.

Trentmann, J., M. O. Andreae, H.-F. Graf, P. V. Hobbs, R. D. Ottmar, and T. Trautmann (2002), Simulation of a biomass-burning plume: Comparison of model results with observations, *J. Geophys. Res.*, *107*(D2), 4013, doi:10.1029/2001JD000410.

Yamasoe, M. A., Y. J. Kaufman, O. Dubovik, L. A. Remer, B. N. Holben, and P. Artaxo (1998), Retrieval of the real part of the refractive index of smoke particles from Sun/sky measurements during SCAR-B, *J. Geophys. Res.*, *103*(D24), 31893–31902.

Zhang, J., S. A. Christopher, and B. N. Holben (2001), Intercomparison of smoke aerosol optical thickness derived from GOES 8 imager and ground-based Sun photometers, *J. Geophys. Res.*, *106*(D7), 7387–7397.

W.-T. Chen, Department of Environmental Science and Engineering, California Institute of Technology, 1200 East California Boulevard, Mail Code 210-41, Pasadena, CA 91125, USA.

R. A. Kahn, NASA Goddard Space Flight Center, Code 613.2, Greenbelt, MD 20771, USA.

D. Nelson and K. Yau, Jet Propulsion Laboratory, California Institute of Technology, MS 169-237, 4800 Oak Grove Drive, Pasadena, CA 91109, USA.

J. H. Seinfeld, Department of Chemical Engineering, California Institute of Technology, 1200 East California Boulevard, Mail Code 210-41, Pasadena, CA 91125, USA. (seinfeld@caltech.edu)